Faculdade de Engenharia da Universidade do Porto



Development of Functional Porous Calcium Phosphate Spheres for Bone Regeneration

Ana Carolina Gregório Pinho

Dissertation developed in the context of the MSc in Bioengineering

Supervisor: Maria Ascensão Lopes
Co-supervisor: José Domingos Santos

September 2022

© Carolina Pinho, 2022

Abstract

Bone is a tissue with a unique healing process since it can regenerate in a way where the original tissue and its pre-existing properties are restored. Nevertheless, if a bone defect exceeds a certain size, this regeneration will not occur spontaneously. Therefore, in some cases, such as critically sized bone defects or non-unions, treatment with bone grafts may be required to assist in the regeneration process. There are plenty of commercially available bone grafts. However, a grafting technique that fully meets the regenerative needs of bone tissue does not exist.

A surgical procedure to implement these types of bone grafts can frequently result in infections and may lead to severe problems such as prolonged hospitalization and, in the worst case, limb amputation. Thus, infections acquired in surgery represent a significant burden associated with such procedures. It is, therefore, essential for a bone graft to have antibacterial properties in order to prevent possible infections.

In the scope of this dissertation and trying to overcome some limitations of the available bone substitutes, it was proposed to develop a system for bone regeneration combining porous hydroxyapatite hollow spheres with an antibiotic (gentamicin) and an osteogenic agent (alendronate), with appropriate characteristics for the release of these drugs. The spheres present a hollow core intended to host the alendronate. In contrast, gentamicin is desired to be adsorbed to the surface of the porous spheres along with gelled alginate. As such, gentamicin and alendronate are intended to have a short-term and a long-term release profile, respectively.

As part of the dissertation's experimental work, it was possible to impart optimal porosity and pore interconnectivity onto the spheres using a surfactant. These properties are essential for bone growth and drug release. Regarding the alendronate and gentamicin release studies, these were initially performed with spheres loaded with both agents and with spheres loaded with only one of the drugs (gentamicin or alendronate). However, it became evident that it was not feasible to quantify the drugs separately by fluorescence spectroscopy since they are detectable at the same excitation and emission wavelengths. Therefore, to have an estimate of the drug release profiles, only the individual assays were quantified. Regarding the gentamicin release profiles, there was an initial burst release, followed by a more controlled drug release over around 16 days, which is ideal in a clinical setting. As for the alendronate release profiles, these have shown to be quite promising as they exhibited a pulsatile pattern for about 24 to 28 days, promoting osteogenic differentiation through stimuli, and displaying a sustained release.

Evaluation of the antibacterial effect of the spheres demonstrated that all spheres loaded with the two agents had an antibacterial effect for *Staphylococcus aureus* for five days.

However, there was a discrepancy between these results and those obtained in the gentamicin release studies, which may be due to the fact that these were performed with double-loaded spheres, and this will differ from the results obtained in the release profiles with spheres loaded only with gentamicin. Moreover, the double-loaded spheres showed no cytotoxicity to MG-63 cells, however, by assessing the cytotoxicity of alendronate itself, it could be seen that it exhibited some cytotoxicity for the concentration range obtained in the alendronate release tests (10^{-4} M to 10^{-5} M).

Therefore, it is possible to state that, although some future work has to be performed in the experimental setting, the system developed in this work exhibited antibacterial and osteogenic properties and possesses the therapeutic potential to be implemented in the context of bone regeneration.

Resumo

O osso é um tecido com um processo de reparação único, uma vez que pode regenerar de forma que o tecido original e as suas propriedades pré-existentes sejam restaurados. Contudo, se um defeito ósseo exceder um determinado tamanho, esta regeneração não ocorrerá espontaneamente. Portanto, em alguns casos, tais como defeitos ósseos de tamanho crítico ou não-uniões, é necessário o tratamento com enxerto ósseo para ajudar no processo de regeneração. Existem muitos enxertos ósseos disponíveis comercialmente. No entanto, não existe uma técnica de enxerto que satisfaça plenamente as necessidades regenerativas do tecido ósseo.

Um procedimento cirúrgico para implementar este tipo de enxertos ósseos pode frequentemente resultar em infeções e pode levar a problemas graves, tais como hospitalização prolongada e, no pior dos casos, amputação de membros. Assim, as infeções adquiridas em cirurgia representam um fardo significativo associado a tais procedimentos. É, portanto, essencial que um enxerto ósseo tenha propriedades antibacterianas, a fim de prevenir possíveis infeções.

No âmbito desta dissertação e tentando ultrapassar algumas limitações dos substitutos ósseos disponíveis, foi proposto desenvolver um sistema de regeneração óssea combinando esferas ocas porosas de hidroxiapatite com um antibiótico (gentamicina) e um agente osteogénico (alendronato), com características apropriadas para a libertação destes fármacos. As esferas apresentam um núcleo oco destinado a incorporar o alendronato. Por outro lado, é desejado que a gentamicina seja adsorvida à superfície das esferas porosas juntamente com o alginato gelificado. Como tal, a gentamicina e o alendronato destinam-se a ter um perfil de libertação a curto e a longo prazo, respetivamente.

Como parte do trabalho experimental da dissertação, foi possível conferir porosidade e interconectividade de poros ideais às esferas utilizando um surfactante. Estas propriedades são essenciais para o crescimento ósseo e a libertação de drogas. Quanto aos estudos de libertação de alendronato e gentamicina, estes foram inicialmente realizados com esferas carregadas com ambos os agentes e com esferas carregadas apenas com uma das drogas (gentamicina ou alendronato). Contudo, tornou-se evidente que não era viável quantificar os fármacos separadamente por espectrofotometria de fluorescência, uma vez que estes são detetáveis nos mesmos comprimentos de onda de excitação e emissão. Portanto, a fim de ter uma estimativa dos perfis de libertação dos fármacos, apenas os ensaios individuais foram quantificados. Quanto aos perfis de libertação de gentamicina, houve um pico de libertação inicial, seguido de uma libertação mais controlada da droga durante cerca de 16 dias, o que é ideal num contexto clínico. Quanto aos perfis de libertação de alendronato, estes revelaram-se bastante promissores, uma vez que exibiram um padrão pulsátil durante cerca de 24 a 28

dias, promovendo a diferenciação osteogénica através de estímulos, e mostrando uma libertação sustentada.

A avaliação do efeito antibacteriano das esferas demonstrou que todas as esferas carregadas com os dois agentes tiveram um efeito antibacteriano para *Staphylococcus aureus* durante cinco dias. Contudo, houve uma discrepância entre estes resultados e os obtidos nos estudos de libertação de gentamicina, o que pode dever-se ao facto de estes terem sido realizados com esferas carregadas duplamente, o que diferirá dos resultados obtidos nos perfis de libertação com esferas carregadas apenas com gentamicina. Além disso, as esferas carregadas duplamente não mostraram citotoxicidade para as células de MG-63, contudo, ao avaliar a citotoxicidade do alendronato em si, constatou-se que este apresenta alguma citotoxicidade para a gama de concentrações obtidas nos ensaios de libertação de alendronato (10^{-4} M a 10^{-5} M).

Assim, é possível afirmar que, embora algum trabalho futuro tenha de ser realizado no âmbito experimental, o sistema desenvolvido neste trabalho apresenta propriedades antibacterianas e osteogénicas e possui o potencial terapêutico para ser implementado no contexto da regeneração óssea.

Acknowledgments

Primeiramente, quero agradecer à minha orientadora, a professora Maria Ascensão Lopes pela confiança, pela compreensão, e por me ter acompanhado e ajudado ao longo deste percurso. Quero também agradecer ao meu coorientador, o professor José Domingos Santos, pelo apoio prestado.

Obrigada ao Miguel Rodrigues por ter tido sempre disponibilidade para me explicar e ajudar na componente laboratorial e por todos os ensinamentos proporcionados ao longo deste semestre. Agradeço também à professora Maria Pia Ferraz por se ter mostrado disponível para me auxiliar nos ensaios bacterianos e à Liliana Grenho por toda a ajuda e orientação prestada nos ensaios celulares.

Obrigada às Catarinas e à Beatriz por toda ajuda e companheirismo no laboratório.

Um obrigado especial aos meus amigos por sempre me ouvirem e apoiarem e por permanecerem ao meu lado durante estes 5 anos de percurso académico. E a todas as pessoas com quem cruzei caminhos durante estes anos e que, de uma forma ou de outra, contribuíram para a pessoa que sou hoje.

Por fim, mas não menos importante, quero agradecer à minha família, principalmente aos meus pais e à minha irmã por serem os grandes pilares da minha vida. Obrigada pela educação e por sempre me ajudarem quando (parece que) as coisas não estão a correr bem. Obrigada, Rafa, por teres sempre uma palavra tranquilizante. Obrigada, pai, por me ensinares que desistir nunca é o caminho e para lutar sempre pelo que quero, mesmo que não seja fácil. Obrigada, mãe, por seres sempre o meu porto seguro e por me conseguires sempre acalmar. Sei que parece cliché, mas sem vocês não chegaria aqui.

Table of contents

Chapter 1: Introduction 17

1.1. Motivation and work proposal 17

Chapter 2: State of the art 18

2.1. Bone function and physiology 18

2.2. Bone healing 19

2.3. Osteoporosis and bone defects 20

2.4. Scaffolds and their crucial features 22

2.5. Bone grafts 23

2.6. Bioceramics 24

2.7. Drug delivery systems for bone regeneration 25
2.7.1. Bisphosphonates 27
2.7.2. Antibacterial agents 28

2.8. Commercially available bone graft substitutes with associated drug release 29

Chapter 3: Materials and Methods 31

3.1. Materials 31

3.2. Methods 32
3.2.1. Production of the hydroxyapatite spheres 32
3.2.1.1. Preparation of the ceramic foam 32
3.2.1.2. Production of the hollow spheres 33
3.2.2. Characterization of the ceramic spheres 35
3.2.2.1. Morphological observation under the stereomicroscope 35
3.2.2.2. Porosity analysis 35
3.2.2.3. Morphology and topography analysis 36
3.2.3. Drug release studies 36
3.2.3.1. Test samples 37
3.2.3.2. Drug loading in the spheres 38
3.2.3.3. Release profiles 39
3.2.3.4. Gentamicin spectrophotometric quantification 39
3.2.3.5. Alendronate spectrophotometric quantification 40
3.2.4. Antimicrobial activity assessment 40
3.2.4.1. Culture medium preparation 41
3.2.4.2. Bacterial suspension preparation 41
3.2.4.3. Mueller Hinton agar diffusion test 42
3.2.5. In vitro biological evaluation 42
3.2.5.1. Cytotoxicity evaluation of the samples 42
3.2.5.2. Cytotoxicity evaluation of the compound 43
3.2.5.3. Resazurin assay 43
3.2.5.4. Cell morphology analysis 43
3.2.6. Statistical analysis 44

Chapter 4: Results and Discussion 45

4.1. Production and characterization of the porous spheres 45
4.1.1. Production of the hollow spheres 45
4.1.2. Heat treatment 46
4.1.3. Morphological observation under the stereomicroscope 46
4.1.4. Morphology and topography analysis 47
4.1.5. Porosity analysis 48

4.2. Drug release studies 49
4.2.1. Drug loading 49
4.2.2. Gentamicin release studies 50
4.2.2.1. Gentamicin release profiles 51
4.2.3. Alendronate release studies 53
4.2.3.1. Alendronate release profiles 54

4.3. Antibacterial activity assessment 57
4.3.1. Mueller Hinton agar diffusion test 57

4.4. *In Vitro* biological evaluation 59
4.4.1. Cytotoxicity evaluation of the samples 59
4.4.2. Cell morphology analysis 61
4.4.3. Cytotoxicity evaluation of the compound 62

Chapter 5: Conclusions and Future Work 65

References 68

List of figures

Figure 1- Structural composition of bone and the three main cells that constitute it. Created with BioRender.com. 19

Figure 2- Bone healing stages [15]. 20

Figure 3- Normal bone (1) and osteoporotic bone (2) due to excessive expression of RANKL. Created with BioRender.com. 21

Figure 4- Schematic representation of drug molecules embedded in the hydrogel matrix. ... 27

Figure 5-Some examples of non-nitrogen-containing and nitrogen-containing BPs. 28

Figure 6- Schematic illustration of the syringe-foaming method to produce the ceramic foam. Created with BioRender.com. 32

Figure 7- Metallic mold with two injection channels, used for the production of the spheres. 33

Figure 8- PHD ULTRA Harvard Apparatus infusion pump with two syringes laid on top. 34

Figure 9- Loading process of the two drugs in the spheres. Created with BioRender.com. ... 38

Figure 10- Placement representation of the spheres in the Petri dishes. Created with BioRender.com. 41

Figure 11- Layout representing the placement of the spheres in the 96-well plate. Created with BioRender.com. 43

Figure 12- Representative stereomicroscope images of the surface (A) and the core (B) of the hydroxyapatite hollow spheres. 46

Figure 13- Representative SEM images of a hollow porous sphere post-sintering at 250x magnification, highlighting its pores and respective diameters measured in ImageJ software (A) and at 100x magnification highlighting the sphere's core and surface (B). 47

Figure 14- Representative SEM image of the hollow sphere after sintering at 100x magnification and the respective core diameter measured in ImageJ software. 48

Figure 15- Gentamicin concentration release profile (a) and cumulative mass percentage of gentamicin released (b) in the 1G and 2G conditions over 28 days. **Erro! Marcador não definido.**

Figure 16- Alendronate concentration release profile (a) and cumulative mass percentage of alendronate released (b) in the 1Al, 3Al and 4Al conditions over 28 days. ..... **Erro! Marcador não definido.**

Figure 17- Bacterial tests on Mueller Hinton inoculated culture plates over 7 days. All dual loading conditions were tested (1G+4Al; 1G+3Al; 2G+1Al and 1G+1Al), as well as non-loaded and alendronate-loaded spheres (NL and 1Al). 58

Figure 18- Cytotoxicity of the 1G+1Al, 1G+4Al, 2G+1Al conditions and non-loaded spheres (control) over 10 days presented in fluorescence arbitrary units. *=p<0.05 between each sample and the control group at each time-point, for N=5. 60

Figure 19- Images obtained using the SEM technique where cell-material interactions can be observed at 2500x magnification. Control group at 24 hours (a) and fourth day (b); 1G+1Al condition at 24 hours (c) and fourth day (d); 1G+4Al condition for 24 hours (e) and fourth day (f); 2G+1Al condition at 24 hours (g) and fourth day (h). 62

Figure 20- Cytotoxicity of different concentrations of alendronate (10^{-4} M, 10^{-5} M,10^{-6} M,10^{-7} M) over 10 days presented in fluorescence arbitrary units. *=p<0.05 between each sample and the control group at each time-point, for N=5. .....**Erro! Marcador não definido.**

List of tables

Table 1- Some commercially available bone substitutes with associated agents. 30

Table 2- Detailed conditions of the dual and individual release tests. 37

Table 3- Loading efficiency of the gentamicin (1G, 2G) and alendronate (1Al, 3Al, 4Al) conditions, determined by fluorescence spectrophotometry. *=p<0.05 between conditions 1G and 2G, for N=6. ¨=p<0.05 among conditions 1Al, 3Al and 4Al, for N=6. . 50

Abbreviations

BMP	Bone Morphogenetic Protein
BPs	Bisphosphonates
Ca^{2+}	Calcium ion
$CaCl_2$	Calcium chloride
DBM	Demineralized Bone Matrix
FGF	Fibroblast Growth Factor
HA	Hydroxyapatite
HPLC	High-Performance Liquid Chromatography
IGFs	Insulin-like Growth Factors
MG-63	Human osteosarcoma cell line
MIC	Minimum Inhibitory Concentration
MSCs	Mesenchymal Stromal Cells
OPA	O-Phthalaldehyde
PDGF-BB	Platelet-Derived Growth Factor
PMMA	Polymethylmethacrylate
RANK	Receptor Activator of Nuclear Factor κB
RANKL	Receptor Activator of Nuclear Factor κB Ligand
rhBMP-2	Recombinant Human Bone Morphogenetic Protein-2
rhPDGF-BB	Recombinant Human Platelet-Derived Growth Factor-BB
RPM	Revolutions Per Minute
SEM	Scanning Electron Microscopy
SSI	Surgical Site Infection
TGF	Transforming Growth Factor
VEGF	Vascular Endothelial Growth Factor
XRD	X-ray Powder Diffraction
α-MEM	Alpha-Minimum Essential Medium
α-TCP	Alpha- Tricalcium Phosphate
β-TCP	Beta-Tricalcium Phosphate

Chapter 1: Introduction

1.1. Motivation and work proposal

With the significant increase in average life expectancy, there will be subsequent aging of the population. It is estimated that the population aged 60 and over is currently seeing faster growth than all younger age groups worldwide, according to data from the World Population Prospects. Musculoskeletal problems such as arthritis and osteoporosis are increasingly common in the elderly population [1]. Therefore, given the increased number of bone disorders, there is an increasing demand for bone grafts and bone substitutes. About 1 million cases of bone defects requiring bone grafting procedures to achieve union and thus normal healing are reported every year in the United States and Europe. Nowadays, the generally used treatments are mainly autografts and allografts. These approaches are the "gold standard" for the repair of extensive or difficult bone injuries, with at least 2.2 million surgeries being performed each year worldwide, yet they present a few disadvantages [2], [3]. A surgical procedure to implement these types of bone grafts can often result in surgical site infection (SSI), an infection that develops in the region where the procedure was done. In orthopedics, these account for about 20 % of all hospital-acquired infections. In addition, osteoarticular infections are generally difficult to treat and associated with lifetime risks of recurrence of about 10-20 %, especially in the case of multi-resistant pathogens. Patients suffering from these infections have considerably higher physical limitations and reduced quality of life [4], [5].

Therefore, in the context of this dissertation and in an attempt to surpass certain limitations of the available bone substitutes, it was suggested to develop a bone regeneration system by combining porous hydroxyapatite hollow spheres with an antibiotic (gentamicin) and an osteogenic substance (alendronate), with suitable characteristics for the release of these drugs. The spheres exhibit a hollow core designed to host the majority of the alendronate. In contrast, gentamicin is intended to be adsorbed to the surface of the porous spheres along with gelled alginate. As such, gentamicin and alendronate are intended to have a short-term and long-term release profile, respectively. The porous spheres are composed of hydroxyapatite, a calcium phosphate with a very similar composition to the mineral phase of bone, which makes them very biocompatible. In addition, their porosity and pore interconnectivity have a favorable influence on the drug loading as well as on cell recruitment and adhesion to the material when implanted [2].

Chapter 2: State of the art

2.1. Bone function and physiology

The skeleton contributes to a variety of essential functions of the human body. It provides structural support, allows movement and locomotion by granting a foundation for the muscles, protects the internal organs, contributes to acid-base balance, serves as a reservoir of growth factors and cytokines, and ensures a suitable environment for hematopoiesis in the bone marrow. Thereby, it is a vital structure in the human body [6].

Bone is a composite compound consisting of an inorganic (mineral) phase, an organic phase, and water. Bones' mineral phase is quite similar to hydroxyapatite. Approximately 90% of the organic phase of bone consists of collagen type I, while non-collagenous proteins constitute about 5% of this phase, and about 2% consists of lipids [7]. The inorganic phase of bone confers mechanical rigidity and load-bearing strength to this tissue, while the organic matrix provides elasticity and flexibility [6].

The structural composition of bone comprises two forms, cortical (compact) bone and trabecular (cancellous) bone. Cortical bone encloses the bone marrow and is denser; therefore, it is characterized by a high torsional resistance compared to trabecular bone. The latter is formed by a loose network of honeycomb-like plates interposed in the bone marrow compartment, with a high surface area and higher elasticity. The adult human skeleton is, in general, composed of 80 % cortical bone and 20 % trabecular bone.

Compact bone has an outer periosteal surface that contains vascular channels, osteoblasts, and osteoclasts, and an inner endosteal surface adherent to the bone marrow [6], [8].

Osteoblasts, osteoclasts, and osteocytes are the three main cell types that constitute bone, as seen in figure 1.

Osteoblasts are bone-forming cells that differentiate from mesenchymal stem cells. These synthesize and secrete bone organic matrix containing type 1 collagen and regulate its mineralization. Osteoblasts can either differentiate into osteocytes, bone lining cells, or go through apoptosis.

Osteoclasts are the cells responsible for resorbing bone. They are multinucleated cells that derive from macrophages. Osteoclasts also contain acids and enzymes that are released to resorb bone.

Osteocytes are differentiated from osteoblasts and constitute more than 90% of adult bone cells. They lie within gaps in the bone matrix and act as an organizer of intracellular communication. Osteocytes can transduce mechanical stimuli into signals that regulate the activities of osteoblasts and osteoclasts. These are also involved in mineral homeostasis where a balance exists between bone formation and bone resorption [8].

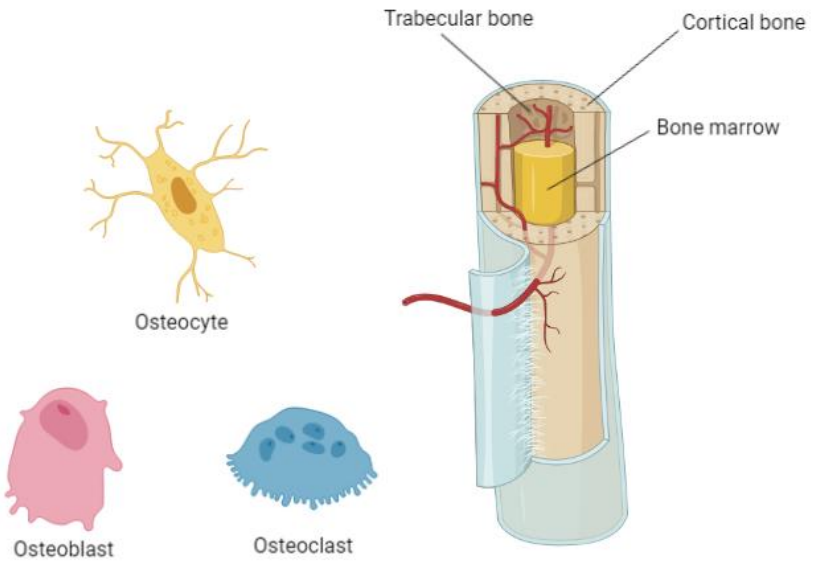


Figure 1- Structural composition of bone and the three main cells that constitute it. Created with BioRender.com.

2.2. Bone healing

Bone tissue has a unique healing process in comparison to other connective tissues as it hosts several cellular and molecular pathways that are able to form new bone rather than a fibrous scar. This feature gives bone tissue the uniqueness of scarless regenerative ability where the original tissue is regenerated, and its pre-existing properties are mostly restored [9]–[11].

The major influencing factors in the bone healing process after a bony injury are the availability of blood supply, mechanical stability, the size of the defect, and the severity of surrounding tissue damage.

Following a bone injury, a healing cascade is engaged to recover the original state of the tissue. This cascade has three main phases: inflammation, repair, and remodeling. The repair phase is divided into two stages, soft callus formation and hard or bony callus formation, as can be seen in figure 2.

The Inflammatory phase consists of a hematoma formation since fibroblasts and cells of the inflammatory cascade (mainly macrophages, lymphocytes, and monocytes) start to migrate to the site of lesion and penetrate the bone, leading to the production of granulation tissue, vascular tissue expansion, and mesenchymal cell migration. This phase can take from hours to days. The inflammatory reaction is related to pain, heat, swelling, and the release of various growth factors and cytokines that have crucial functions in repair [10], [12], [13].

Regarding the repair phase, a collagen matrix is deposited and osteoid is secreted and mineralized. These merge to become a soft callus around the injured site, lasting between 4 to 6 weeks. During this phase, angiogenesis, which involves the formation of new blood vessels

from existing ones, also takes place. As the soft callus ossifies, a disorganized structure known as woven bone is gradually formed.

Throughout the remodeling stage, this disorganized structure mentioned previously is eventually reshaped into trabecular bone. This restructuring takes place in turn to mechanical stresses signaled to osteocytes and subsequently osteoclasts and osteoblasts. Therefore, under ideal conditions, the repair mechanism constantly improves the characteristics of bone by remodeling this tissue through osseous deposition and resorption [12], [13].

In a typical setting, osteoclasts are responsible for disintegrating bone, and, on the other hand, osteoblasts are in charge of its formation. This phenomenon allows the efficient repair of bone defects from regular daily activity, maintains bone mechanical strength, and ensures calcium phosphate homeostasis. Nevertheless, the function designated to osteoclasts can overlap that of osteoblasts, which results in a loss of bone mass and density and an increased bone fragility, thus making it more susceptible to fractures. This can occur, for instance, in an osteoporotic scenario [6], [14].

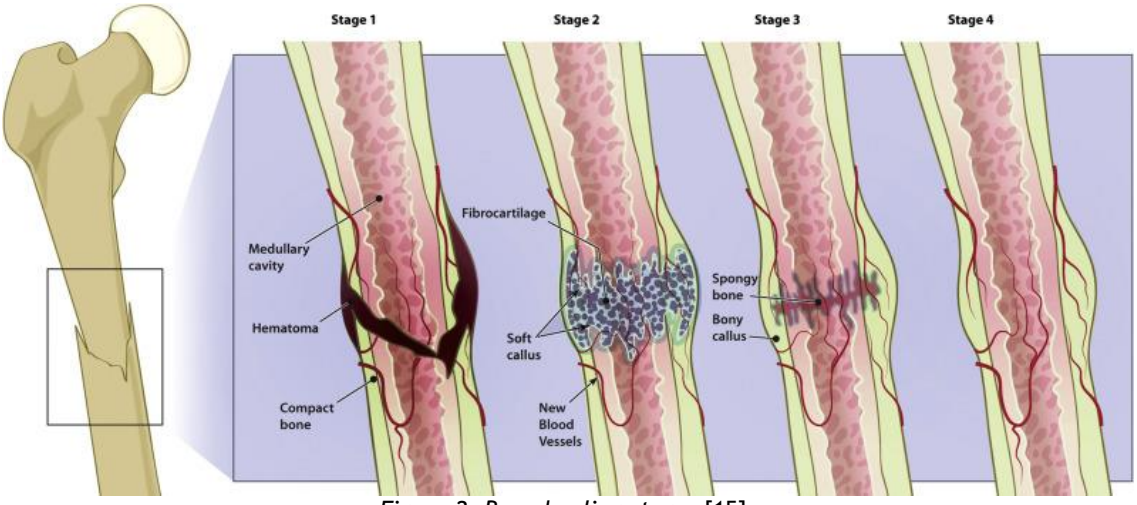


Figure 2- Bone healing stages [15].

2.3. Osteoporosis and bone defects

Osteoporosis is the most common chronic skeletal disorder characterized by low bone mass, deterioration of bone tissue, and disruption of bone microarchitecture, which consequently reflects in bone density and quality. Due to this disorder, the trabecular bone loses mass. As a consequence of a reduction in the connection points, the bone will become more brittle, leading to increased fracture risk [14], [16], [17].

As previously mentioned, osteoporosis is a consequence of a superior action of osteoclasts compared to osteoblasts. Furthermore, hormones such as estrogen, parathyroid hormone, and testosterone also strongly influence bone remodeling. When the levels of these hormones are unbalanced, for instance, during menopause, the rates of bone resorption and

formation drastically change, leading to osteoporosis. Therefore, it is a very prevalent condition in postmenopausal women [14].

The receptor activator of nuclear factor κB ligand (RANKL) also influences bone remodeling. This molecule is secreted by osteoblasts and triggers its receptor, RANK, which is expressed on osteoclasts. Once RANK is activated, there is a proliferation and activation of osteoclasts, resulting in deep bone resorption [18], as illustrated in figure 3.

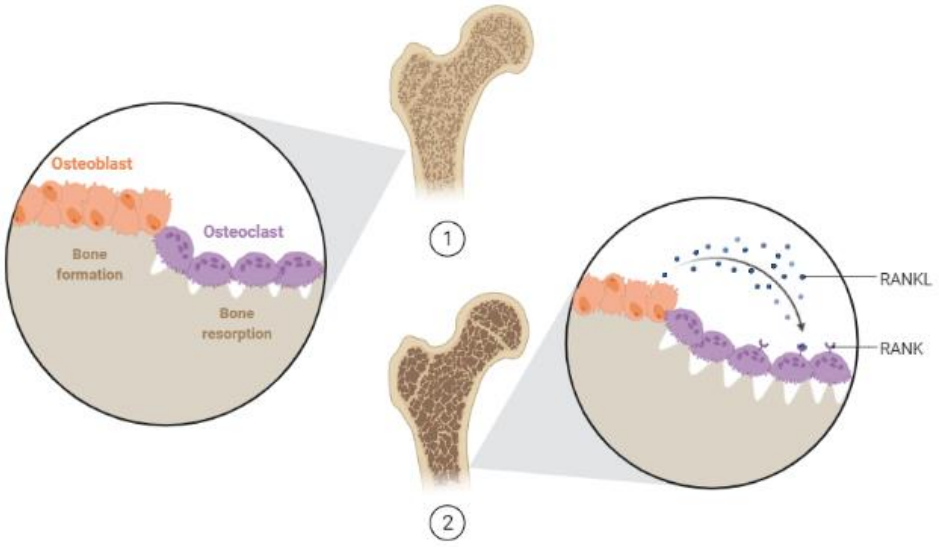


Figure 3- Normal bone (1) and osteoporotic bone (2) due to excessive expression of RANKL. Created with BioRender.com.

A bone fracture consists of a partial or complete disruption in the anatomical continuity of bone, causing it to become mechanically unstable. It is usually associated with damage to the surrounding tissues, including blood supply, and in most cases results in an impaired function of the locomotor system. Fractures are often associated with falls, car accidents, sports injuries, and other factors such as insufficient bone density associated with osteoporosis.

Fractures can be closed, with no skin rupture, or open, involving skin rupture. The later ones are associated with more damage to the surrounding tissues and carry a higher risk of infection and non-union [19].

Currently, the management related to bone defects remains a significant burden, especially if it involves a critically sized bone defect. There is no standard definition of these defects, as they may vary depending upon many factors. The defects can be assessed both in relative and absolute terms. Overall, a "critical size" defect is regarded as a defect that would not heal spontaneously despite surgical stabilization and requires further operative intervention [20]. Some parameters are suggested in the literature, such as defect lengths longer than 1-2 cm and more than 50% bone circumference loss. Nevertheless, this is in part influenced by the anatomical location of the defect and the condition of the surrounding soft tissue. It is also essential to distinguish a non-union from a critical size defect. In the first case, there is impaired cellular and molecular signaling and biomechanical instability. In contrast, in the second case, there is often adequate biology but a failure to replace a substantial bone

loss that may be further complicated by the soft tissue surroundings. Furthermore, a critically sized bone defect will always demand management of the defect, while a non-union may or may not require treatment with a bone graft [20].

2.4. Scaffolds and their crucial features

Every tissue is composed of a matrix containing one or more cell types. This matrix supplies a tissue-specific environment and architecture to the cells and works as a reservoir for nutrients, water, cytokines, and growth factors. Hence, to regenerate and restore a particular tissue, a template (scaffold) is required as a temporary matrix for cell proliferation and extracellular matrix deposition to achieve tissue growth until its complete regeneration. An appropriate 3D scaffold is therefore essential for a tissue engineering strategy. Nevertheless, it is essential to understand that the latter must comply with various properties and requirements that make it suitable for tissue engineering purposes [2].

Evidently, any scaffold used in tissue engineering must be biocompatible. This property translates into the ability of a material to perform its desired function with respect to a medical therapy, without causing any undesirable local or systemic effects to human tissues [21].

When it comes to bone tissue engineering, the porosity of a scaffold is a major factor. Porosity is defined as the percentage of voids in a solid material. Pores are essential for bone tissue formation since they enable the migration and proliferation of osteoblasts and mesenchymal cells, as well as tissue vascularization and angiogenesis [22]. Scaffolds should have a fully interconnected geometry in a highly porous structure with a wide surface area in order to promote neovascularization from the neighboring tissue, as well as cell proliferation and distribution throughout the construct [23]. Furthermore, scaffolds should also exhibit adequate microporosity (pore diameter < 20 μm). Studies have suggested that this property contributes to bone ingrowth by increasing the surface area for protein adsorption, while also providing anchoring points for osteoblasts and allowing capillary ingrowth. On the other hand, macroporosity (pore diameter > 50 μm) is believed to assist osteogenesis by allowing the transport of cells and ions [2], [24]. Porosity and interconnectivity are also significant for an accurate diffusion of nutrients and gases in deeper areas and the removal of metabolic waste resulting from cell activity. Nevertheless, porosity rate should always be adjusted with the mechanical requirements of the specific tissue that is to be replaced since it affects other scaffold features, such as mechanical stability and the scaffold’s degradation rate [2].

Another essential property of scaffolds for bone tissue engineering is osteoconductivity. This is defined as the ability to provide a 3D matrix for the migration of capillaries, tissues, and osteoprogenitor cells into the graft [25]. Since bone is always under tension *in vivo*, it is also important to consider the construct's mechanical characteristics. These need to ideally mimic the bone's properties where the scaffold will be implanted. Furthermore, the degradation rate of the scaffold must be properly adjusted to the rate of new tissue growth,

in such a way that as the tissue is being regenerated, the scaffold is being controllably degraded [2].

2.5. Bone grafts

Bone grafting has been used by orthopedic surgeons for many years to assist in the bone healing process when the defect is unable to heal spontaneously, as in the case of the critical size bone defects previously mentioned. Furthermore, complications such as delayed union, non-union, and malunion also frequently require bone grafts, and these can also be used to fill bone defects caused by tumors. Bone grafts can be categorized into four major groups: autografts, allografts, xenografts, and synthetic bone graft substitutes. Xenografts are frequently employed in dentistry and originate from a different species than the graft receptor. However, the usual treatments employed nowadays are mainly autografts and allografts. These approaches are the "gold standard" for the repair of extensive or difficult bone injuries, with at least 2.2 million surgeries being carried out every year worldwide. Bone grafts vary with regard to their osteoconduction, osteoinduction, osteogenesis, and structural support characteristics [3], [26]. Osteoconduction, as previously discussed, is a process whereby a graft serves as a scaffold, passively harboring the cells required for bone repair, such as mesenchymal stem cells, osteoblasts, and osteoclasts. On the other hand, the ability of a bone graft to recruit, proliferate, and differentiate mesenchymal stem cells into osteoblastic cells represents its osteoinductive ability. In turn, osteogenic bone grafts already possess all the cellular and growth factors while being a scaffold to form new bone [26].

An autologous bone graft is one that is collected from one anatomical place and transferred to another within the same individual. This type of graft is considered the “gold standard” procedure in bone grafting as it possesses excellent osteoconduction, osteoinduction (due to the presence of growth factors), and osteogenic properties (owing to the presence of living osteogenic cells), which ultimately translates into a faster and more complete integration into the host bone. Nevertheless, autografts have many drawbacks primarily associated with harvesting, including donor site complications, increased blood loss, extended operative time, potential donor site infection, and limited volume of available tissue [27].

Bone allograft refers to bone tissue that is harvested from one individual and transplanted to another individual of the same species. This graft is most of the times of cadaveric origin and is available in trabecular or cortical forms as well as demineralized bone matrix (DBM). Even though most allografts are osteoconductive, DBM has the advantage of exhibiting osteoinductive properties. The DBM consists of a bone matrix containing collagen, non-collagenous proteins, and growth factors conferring osteoinductive properties to this graft. Allografts address some drawbacks of autogenous grafts. These are available in larger quantities and are not associated with morbidity at the donor site. However, allografts lack

the optimal integration with the surrounding tissues of autogenous grafts, have poor bioactivity, the chance of donor rejection, and the possibility of transmission of pathogens and infection [26], [27].

When it comes to synthetic bone grafts, it can be stated that they only possess osteoconduction properties when compared to allografts and autografts. In addition, synthetic bone grafts must be biocompatible, undergo remodeling, and bear new bone formation. Mechanically, they should have similar strength and elasticity modulus as cortical or trabecular bone, depending on the site to be implanted [28].

The most commonly used materials for this type of bone graft are bioceramics, such as calcium sulfate, calcium phosphate, tricalcium phosphate, and hydroxyapatite, thus providing an osteoconductive scaffold to promote bone deposition. Composite bioceramics are also available, using a combination of the ceramics mentioned above to achieve optimal properties. Such materials can potentially eliminate some complications and limitations of the “gold standard” grafts. However, they have neither osteogenic nor osteoinductive properties [26].

2.6. Bioceramics

Calcium phosphate-based ceramics are appealing materials for bone tissue regeneration. This is because their composition is remarkably comparable to the mineral component of natural bone. The ones conceived to interact with biological tissue are referred to as bioceramics. Bioceramics can be classified based on the extent to which they react with biological tissues and are therefore divided into inert, bioactive, and biodegradable. Inert bioceramics can trigger a foreign body reaction upon contact with bone tissue, which accounts for the loss of many implants. Consequently, more research has been devoted to bioactive and biodegradable ceramics [29].

Biodegradable bioceramics are intended to perform certain functions over a specific period, assisting in bone repair and resorbing as new bone is formed. However, it should be noted that one limitation of such ceramics is their relatively high degradation rate, accompanied by a loss of their mechanical properties, in comparison to the slower process of bone formation [29].

Bioactive bioceramics are so called as they have the ability to couple with bone and favor the formation of bone tissue. The similarity between these materials' surface and structural composition and the bone mineral phase leads to this property. Bioactive ceramics exhibit osteoconductive qualities, promoting bone cell growth and direct bone deposition on their surfaces. Hence, such ceramics have been employed as bony filler material to provide a scaffold for cell migration and rapid bone formation [30].

Good examples of biodegradable bioceramics are tricalcium phosphates (α-TCP or β-TCP). Likewise, an example of a bioactive bioceramic is hydroxyapatite (HA). These are the

most commonly employed calcium phosphate ceramic forms in the bone regeneration field. Specific compositions of glass and glass-ceramics are also commonly used for this purpose. However, the low mechanical strength of calcium phosphates and silica-based bioceramics is a significant drawback. Therefore, they show promising characteristics for repairing bone abnormalities, but only in non-load-bearing sites [29], [30].

HA ($Ca_{10}(PO_4)_6(OH)_2$) has been the most studied calcium phosphate in this area, owing to its high chemical and structural resemblance to the inorganic component of bone, as mentioned above, mainly since its calcium to phosphorus ratio is similar to that of natural bone. Therefore, this material shows high biocompatibility, bioactivity, and osteoconductivity. Published studies have demonstrated the ability of HA to promote new bone tissue formation *in vivo*. Given the different compositions of HA and tricalcium phosphates (TCP - $Ca_3(PO_4)_2$), following implantation of these materials, a different biological response will be induced at the bone defect site. Since hydroxyapatite is thermodynamically more stable at physiological pH and body temperature, it resorbs slower than tricalcium phosphates. As a result, it has less *in vivo* tissue interaction than tricalcium phosphates [29], [31]. However, some calcium phosphates, like α-TCP, react excessively fast, which is a disadvantage when it comes to filling bone defects. Biphasic combinations of HA and TCP were researched to adjust the reaction kinetics dictating the resorption rate of a scaffold. For example, biphasic calcium phosphates with different HA:TCP ratios have been developed for a higher or lower reabsorption rate. Thus, combining the excellent biocompatibility properties of hydroxyapatite with a resorption rate adjusted to the intended application [31].

Bioglasses also fall into the bioceramics category and are widely used in bone regeneration. Among them, Bioglass® 45S5 (45% SiO_2 24.5% NaO_2, 24.5% CaO, and 6% P_2O_5) is the most widely used within this class. These bioceramics exhibit high porosity as well as osteoconductive, osteoinductive, and bioactive properties. Today, the most promising application of bioactive bioglass is in bone tissue engineering as 3D scaffolds in association with osteogenic agents [29], [31].

2.7. Drug delivery systems for bone regeneration

Extensive biological mechanisms, such as cell proliferation, mineralization, and the transport of signaling molecules, such as growth factors, are required for an optimal bone regeneration process. As a result, current regeneration techniques are increasingly incorporating local administration of bioactive substances, such as drugs and growth factors, to replicate these intricate processes. Systemic and local routes are the two main categories in which drug administration pathways can be divided. Drug administration in the classic systemic route occurs through the circulatory system, and can have several negative effects, including systemic toxicity, adverse side effects, and ineffective delivery to the targeted

region. However, local drug delivery techniques overcome some of these limitations, with few adverse effects, significant concentrations in the target tissue, and low systemic absorption.

Additionally, a controlled local release system enhances the drug release kinetics by supplying the required dosage at a regulated rate and time (from hours to years), safeguarding the drugs from environmental factors like degradation, and boosting therapeutic efficacy [32].

The prevention of bone infections is a considerable challenge in bone surgery. The development of serious complications such as prolonged hospitalization or poor functional outcome brought on by postoperative infection associated with the implantation or replacement of a prosthesis or osteoconductive material typically necessitates additional surgery, such as the removal of the device or even amputation of the limb. Therefore, due to this emergent issue, drugs such as antibiotics and anti-inflammatory agents are significant for the success of tissue regeneration therapy. Antibiotic administration is key to reducing the chances of infection during a surgical procedure. In turn, anti-inflammatory drugs will reduce inflammation at the scaffold implantation site, promoting enhanced healing of damaged tissues [33], [34]. Therefore, these compounds are being increasingly used in calcium phosphate scaffolds for local release systems. This targeted approach has also been extensively used with bone growth factors, especially members of bone morphogenetic protein (BMP), vascular endothelial growth factor (VEGF), transforming growth factor (TGF), fibroblast growth factor (FGF), and insulin-like growth factors (IGFs), thus increasing the osteogenic potential of bone substitutes. Along with these growth factors, calcium phosphates have also been widely researched as potential vehicles for the local delivery of bisphosphonates. Bisphosphonates are commonly used to treat conditions like osteoporosis as they successfully enhance bone density and have osteogenic characteristics [33].

Regarding the process of drug loading into a scaffold, it can be achieved by directly mixing the drug with the scaffold material before fabrication, by binding with a drug carrier and adding this system to the scaffold material, by impregnating the drug into the produced scaffold, and lastly, by coating the fabricated scaffold with a polymer or hydrogel [32]. Hydrogels have been widely studied for drug delivery applications due to their unique physical properties. Their highly porous structure can be easily tuned by controlling the bonds within the gel matrix. Additionally, because of their porosity, drugs may be loaded into the gel network (figure 4) and then released at a pace that depends on the diffusion coefficient of the drug molecules in the gel mesh. Effectively, the benefits of hydrogels for drug delivery may be primarily linked to release kinetics concerns, such that the drug slowly elutes, maintaining a high local drug concentration in the desired tissues over a sustained period. However, they can also be used for systemic delivery [35].

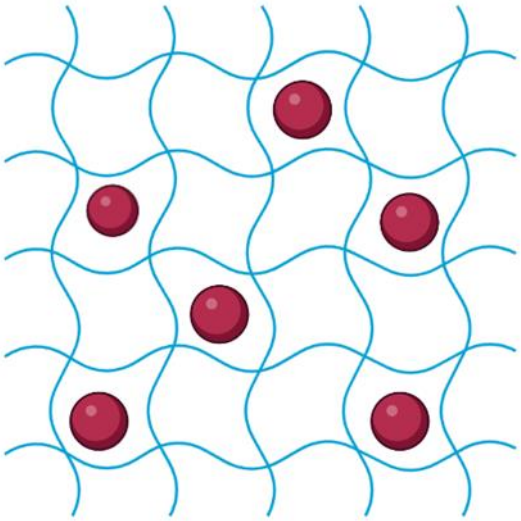


Figure 4- Schematic representation of drug molecules embedded in the hydrogel matrix.

2.7.1. Bisphosphonates

Bisphosphonates (BPs) are the most commonly used agents to address conditions characterized by extensive osteoclast-induced bone resorption. These agents can disturb the bone resorption process and cause osteoclasts' death, thus reducing the loss of bone mass. The chemical structure of bisphosphonates determines the precise processes by which they function. Based on the presence of nitrogen in their chemical composition, these compounds can be categorized into nitrogen-containing or non-nitrogen-containing bisphosphonates (figure 5) [36], [37]. Compared to bisphosphonates without nitrogen, the efficacy of bisphosphonates containing nitrogen, including alendronate, has undoubtedly increased within 10 to 10,000.

These drugs have a particularly strong affinity to bone hydroxyapatite, which causes bisphosphonates to accumulate close to osteoclasts in newly formed bone. The osteoclast microenvironment becomes extremely acidic during the resorption phase, which can encourage the release of bisphosphonates from the bone surface and enhance the local concentration of these substances on the bone mineral surface, particularly near the location of osteoclast activity. Each bisphosphonate has its mechanism of action. The metabolic waste products of bisphosphonates that do not contain nitrogen are toxic and lead to cell death, thus resulting in osteoclast apoptosis. In contrast, nitrogen-containing bisphosphonates attach to and inactivate the enzyme farnesyl diphosphate synthetase, thus resulting in reduced cell function and subsequent cell death. Therefore, non-nitrogen-containing bisphosphonates are less frequently prescribed to patients as they exhibit more harmful effects than nitrogen-containing bisphosphonates [36]. Despite their pharmaceutical efficacy, all drugs of the bisphosphonate class have a few inconveniences that include poor oral bioavailability (1 %-3 %), and side effects of acute gastrointestinal conditions such as gastric ulceration. Such substances are also poorly

absorbed from the gastrointestinal tract. Thus, these limitations have driven the investigation of new targeted delivery systems for bisphosphonates to obtain target-site delivery and reduce their side effects [36], [38].

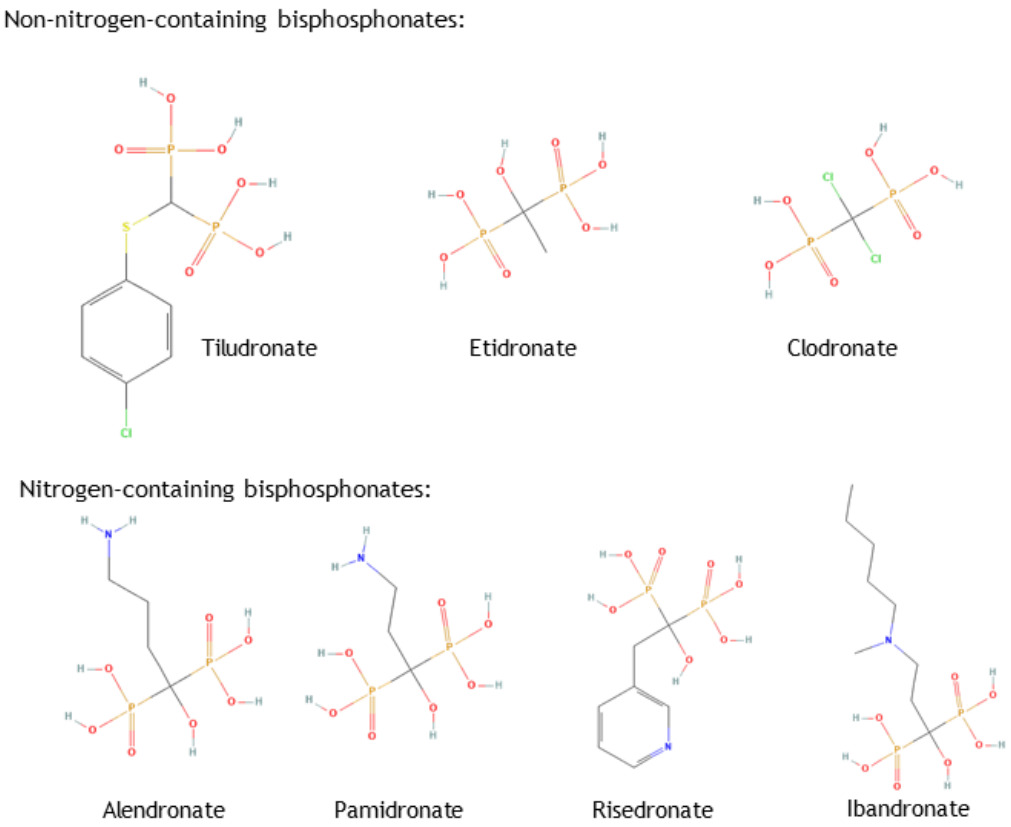


Figure 5-Some examples of non-nitrogen-containing and nitrogen-containing BPs.

2.7.2. Antibacterial agents

The main struggle in orthopedic surgeries is dealing with bone infections caused by bacterial colonization and biofilm development on the implanted device, which impairs the drug performance and body immunity efficacy, thus delaying the bone regeneration process. Furthermore, drug resistance induced by the overuse of antibiotics can lead to even more severe infections. Antibiotics are the most widely used and effective antibacterial therapy for treating bone infections brought on by implantation, and systemic administration is extensively employed in clinics to induce the desired antibacterial effects. Since systemic administration can lead to severe side effects and bacterial resistance, it is crucial to use a local antibacterial strategy, incorporating a potentially antibacterial function into a bioceramic-based scaffold to eliminate the risk of postoperative infection and thereby counteract the side effects of systemic administration of these agents [39].

Antibacterial agents must meet some specific requirements in order to be employed in a local release system. They must release locally at doses above the minimum inhibitory

concentration for the involved bacteria and have an action against the pathogens most often associated with bone infections. Moreover, these agents should not cause adverse effects or enter the systemic circulation and must be stable at body temperature. Some examples of antibiotics that are most commonly employed in addressing bone infections are doxycycline, tetracycline, levofloxacin, ciprofloxacin, and vancomycin [39], [40]. Gentamicin is also a very successful aminoglycoside antibiotic for the management of bone infections and acts by binding to the bacterial 30S ribosomal subunit. Ultimately, this leads to impaired protein synthesis, a buildup of truncated proteins, and bacterial cell death. This antibiotic has a wide spectrum of activity against gram-positive and gram-negative bacteria, such as *Staphylococcus aureus* or *Pseudomonas aeruginosa*, respectively. These two pathogens are often associated with complex bone infections [41], [42].

2.8. Commercially available bone graft substitutes with associated drug release

Some commercially available biomaterials are being used for bone tissue regeneration while preventing surgical site infections, such as polymethylmethacrylate (PMMA) bone cements. These can be employed on their own or with the addition of drugs, such as antibiotics, serving as both bone spacers and local antibiotic delivery systems, and increasing target tissue concentrations while reducing toxicity hazards. This approach, although being one of the most regularly used, has several drawbacks, including a lack of biodegradability and poor drug release kinetics. Besides the often faster than desired drug release, one of the significant disadvantages of these cements is the inadequate cement degradation rate compared to the regeneration rate. Furthermore, PMMA has no inherent adhesive properties and lacks the ability to be osteoinductive or osteoconductive [43], [44].

Furthermore, materials containing osteogenic agents are also found on the market. Although such materials exhibit osteogenic properties, they also have disadvantages and significant side effects related to the administration of growth factors *in vivo*, including surgical site inflammation and ectopic bone formation. This type of materials also exhibits an inadequate release rate, with complete depletion of the substance incorporated occurring too fast [45].

Table 1 provides some examples of bone substitutes combined with growth factors, proteins, and antibiotics that are commercially available.

The system that was proposed to be developed in this dissertation aims to combine the good properties of calcium phosphate-based biomaterials for bone regeneration with a controlled release system of an antibiotic and an osteogenic agent to accelerate the bone regenerative process. As such, gentamicin and alendronate were the selected drugs for this study. They are desired to have a short-term and a long-term release profile, respectively, in

an attempt to overcome the inadequate degradation/regeneration rate and the inappropriate drug release pattern of the commercially available bone substitutes.

Table 1- Some commercially available bone substitutes with associated agents.

Product	*Company*	*Composition*	*Incorporated agent*	*References*
Infuse®	Medtronic	Absorbable collagen sponge carrier	Recombinant human bone morphogenetic protein-2 (rhBMP-2)	[45], [46]
Augment®	Wright Medical Group	Collagen/tricalcium phosphate composite	Platelet-derived growth factor (PDGF-BB)	[46]
GEM 21S®	Lynch Biologics	B-tricalcium phosphate matrix	Recombinant human platelet-derived growth factor-BB (rhPDGF-BB)	[45]
Healos®	OraPharma	Hydroxyapatite	Bovine collagen	[47]
Collagraft®	Zimmer	Hydroxyapatite and tricalcium phosphate	Bovine collagen	[47]
(Genta) C-ment®	Leader Biomedical	PMMA bone cement	Gentamicin	[48]
*PALACOS® +G**	Heraeus Medical	PMMA bone cement	Gentamicin	[49]
CMW1-G®	DePuy Synthes	PMMA bone cement	Gentamicin	[50]
PALAMED® G	Heraeus Medical	PMMA bone cement	Gentamicin	[51]
Simplex®	Stryker	PMMA bone cement	Trobamycin/ Gentamicin	[52]

Chapter 3: Materials and Methods

3.1. Materials

Hydroxyapatite powder ($Ca_{10}(PO_4)_6(OH)_2$; SKU: 501203; CAS number: 12167-74-7) was acquired from Fluidinova. Sodium alginate ($(C_6H_7O_6Na)_n$; Mw= 10000 - 600000 g/mol; CAS number: 9005-38-3) was obtained from PanReac AppliChem. Pluronic F-127 ($(C_3H_6O.C_2H_4O)_x$; CAS number: 9003-11-6; SKU: P2443) and calcium chloride ($CaCl_2.2H_2O$; Mw= 147.01g/mol; CAS number: 10035-04-8; SKU: C8106) were both acquired from Sigma-Aldrich. Sunflower oil was obtained from Fula. Acetone (C_3H_6O; Mw= 58.08 g/mol; CAS number: 67-62-1) was obtained from VWR Chemicals. Alendronate sodium trihydrate ($C_4H_{12}NNaO_7P_2.3H_2O$; Purity: >97.0%; CAS number: 121268-17-5; Mw= 271.08 g/mol) and gentamicin sulfate salt ($C_{60}H_{125}N_{15}O_{25}S$; CAS number: 1405-41-0; SKU: G3632) were acquired from Tokyo Chemical Industry and Sigma-Aldrich, respectively. Methanol (H_3COH; CAS number: 67-56-1) was acquired from VRW Chemicals, o-Phthalaldehyde ($C_8H_6O_2$; Mw=134.13 g/mol; CAS number: 643-79-8), 2-Mercaptoethanol (C_2H_6OS, MW: 78.13 g/mol, CAS number: 60-24-2), Boric Acid (H_3BO_3, MW: 61.83 g/mol, CAS number 10043-35-3) and Potassium Hydroxide (KOH, MW: 56.11 g/mol, CAS number: 1310-58-3) were obtained from Sigma-Aldrich. Mueller Hinton agar (CM0337) was acquired from Oxoid Microbiology Products. Minimum essential medium (REF: 11900-073), antibiotic-antimycotic (REF: 15240-062) and heat inactivated FBS (REF: 10500-064) were all acquired from Gibco. Resazurin sodium salt ($C_{12}H_6NNaO_4$; CAS number: 62758-13-8) was obtained from Sigma-Aldrich. Phosphate buffered saline was obtained from Fisher BioReagents, glutaraldehyde 25% EM-500 mL (REF: G002) was acquired from TAAB Laboratories Equipment and cacodylic acid sodium salt trihydrate 98+% ($(CH_3)_2AsO_2NA.3H_2O$; CAS number: 6131-99-3) was obtained from Thermo Scientific.

3.2. Methods

3.2.1. Production of the hydroxyapatite spheres

The experimental activities performed along the dissertation were initiated with the production of porous hydroxyapatite hollow spheres. The spheres were produced using a droplet technique of a ceramic foam containing hydroxyapatite.

The extruded spheres were subjected to a cross-linking process in a calcium chloride solution and were subsequently dehydrated and sintered.

3.2.1.1. Preparation of the ceramic foam

In order to obtain the ceramic foam, the syringe-foaming technique was used. This method required two connected syringes, a previously prepared ceramic suspension, and a surfactant (Pluronic F-127). The surfactant was used to impart the desired micro and macro porosity onto the spheres.

The ceramic suspension was prepared by mixing 16 mL of sodium alginate 2 % (w/v) with 6 g of hydroxyapatite powder until a viscous and homogeneous slurry was obtained.

Figure 6 provides a schematic representation of the syringe foaming method. Regarding this method, two syringes were attached with a three-way stopcock connector, one containing 2.5 mL of air and the other 3.5 mL of Pluronic F-127 10 % (w/v). The syringes were alternatively pumped until a foam volume of 6 mL was obtained.

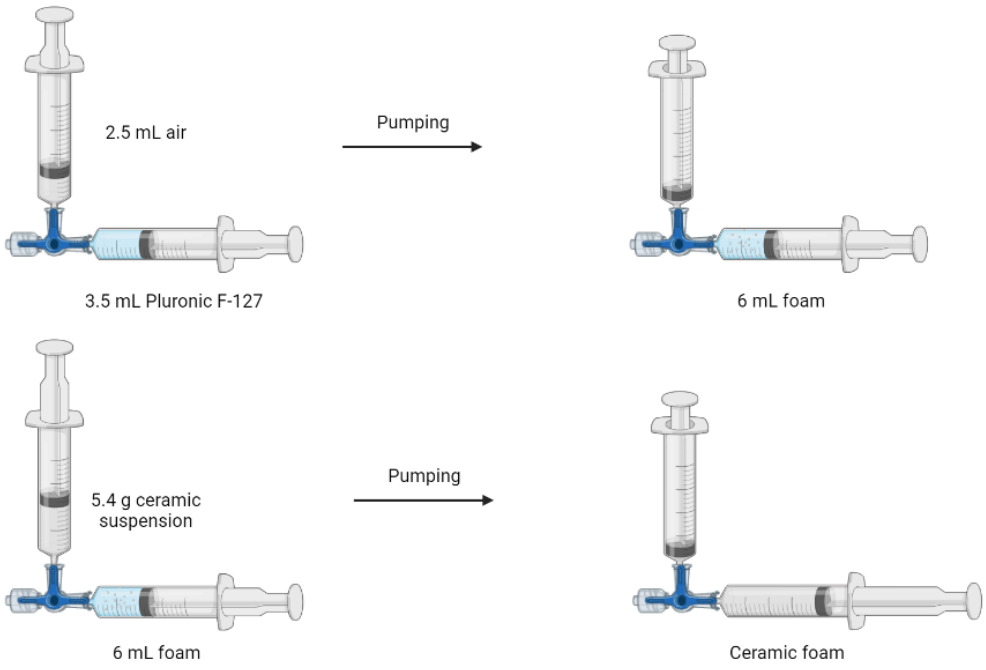


Figure 6- Schematic illustration of the syringe-foaming method to produce the ceramic foam. Created with BioRender.com.

The process was then repeated using 5.4 g of the previously prepared ceramic suspension along with the foam. The syringes were pumped staggered to homogeneously mix the foam with the ceramic slurry, until a volume of about 8 mL was obtained. Thus, a ceramic foam was obtained for the production of the porous spheres.

3.2.1.2. Production of the hollow spheres

Regarding the actual production of the porous and hollow spheres, a co-injection method was implemented. Here, the ceramic foam and sunflower oil were injected into the same metallic mold (figure 7) in separate channels by means of two infusion pumps. The syringes containing the sunflower oil and the ceramic foam were coupled to the mold through channels 1 and 2, respectively.

The sunflower oil was injected into channel 1 and will be responsible for making the hollow sphere core. Conversely, the ceramic hydroxyapatite foam was injected into channel 2 in order to produce the outer layer of the sphere, as can be seen in figure 7.

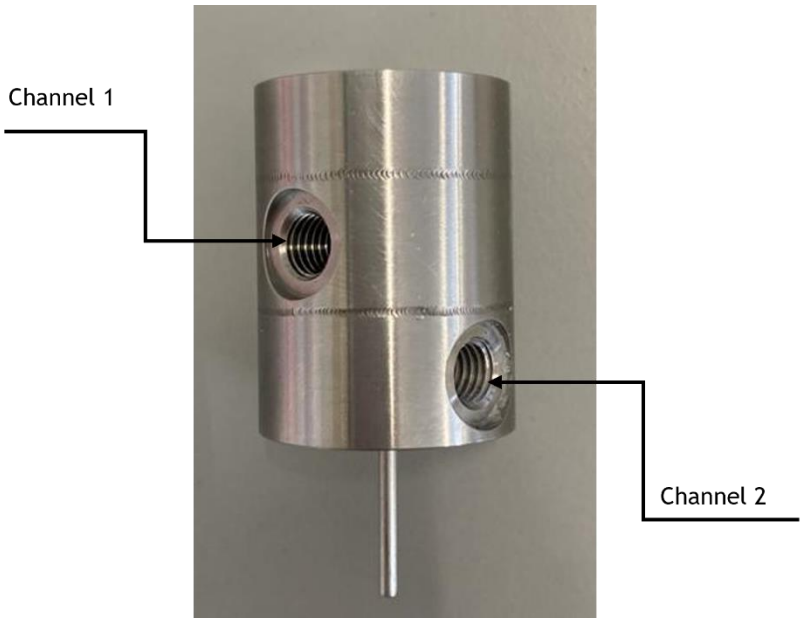


Figure 7- Metallic mold with two injection channels, used for the production of the spheres.

The mold was then placed in a universal holder, adjusted to ensure that the syringes were laid on the infusion pumps, as shown in figure 8, and attached to the holes in the mold, simultaneously.

Following that, the injection flow rate of the two syringes was selected. The sunflower oil injection flow rate was set at 0.2 µL/s. As for the injection flow rate of the ceramic foam, initially it was set at 5 µL/s. Once the foam starts to drop from the mold, the flow rate was adjusted to 1.5 µL/s.



Figure 8- PHD ULTRA Harvard Apparatus infusion pump with two syringes laid on top.

As the spheres were being ejected from the mold, they were dropped into a recipient containing a 1 % (w/v) calcium chloride ($CaCl_2$) solution in order to undergo a cross-linking process.

The spheres remained in the calcium chloride solution for about 30 minutes before undergoing the dehydration process. Here, the spheres were removed from the calcium chloride solution and transferred to a container with acetone for about 2 hours prior to heat treatment. Dehydrating the spheres was important to achieve a better control in the heat treatment cycle. If the spheres were not dehydrated before the heat treatment, their shrinkage rate would be higher than desired.

3.2.1.3. Heat treatment

After dehydration, the spheres were displayed on appropriate supports and placed in the furnace. Here they underwent a heat treatment cycle. During the first heat treatment phase, there was a complete combustion of the organic compounds present in the spheres, namely the sunflower oil and the Pluronic F-127, at 700 ºC. The surfactant combustion was responsible for the pore formation in the spheres. Additionally, the sunflower oil was selected since it is hydrophobic and immiscible with the ceramic foam, thus, it was responsible for the formation of the hollow core after the first phase of the heat treatment. Regarding the sintering of the hydroxyapatite itself, it occurred in the last phase of the cycle, at 1300 ºC.

The sintering process is intended to densify and aggregate the particles within the spheres through the application of heat [53]. Therefore, the process started with increasing the furnace temperature to 700 ºC at a heating rate of 0.5 ºC/min, which was maintained for 2 hours to promote the combustion of the organic compounds. The temperature was then increased again to 1300 ºC at a heating rate of 4 ºC/min, and the furnace remained at this temperature for 3 hours. This was where the sintering of the hydroxyapatite occurred. The cycle was completed by the natural cooling of the spheres still inside the oven.

3.2.2. Characterization of the ceramic spheres

3.2.2.1. Morphological observation under the stereomicroscope

The morphology of the spheres was investigated using a computer-connected Leica stereomicroscope (Leica S7 E). These were cut with a blade to allow for the examination of their hollow interior and porosity.

The stereomicroscope observation was a method of ensuring the batch-level quality of the manufactured spheres, by assessing the core's porosity and concentricity.

3.2.2.2. Porosity analysis

The porosity of the spheres' shell was determined using Archimedes' principle. For each test, three spheres were used, whose diameters (d) were measured using a caliper. These tests were performed with broken in half spheres since it was intended to evaluate only the spheres' shell porosity.

The geometric density (ρ_g) of the spheres was then obtained through the formula:

$$\rho_g = \frac{m}{v} = \frac{m}{\left({}^{4}/_{3}\,\pi r^{3}\right)}$$

where, m and v represent the mass and volume of the sphere, respectively, and $r = \frac{d}{2}$.

Since the spheres have a hollow core, their volume was determined by the following equation:

$$v = v_{theoretical} - v_{core}$$

where $v_{theoretical}$ represents the total volume of the sphere and v_{core} represents the sphere's core volume. The core volume of the spheres was not considered, because the intention was to evaluate the porosity of the spheres' shells only. The core volume was estimated from the core diameter measured by scanning electron microscopy.

The Archimedes density (ρ_a) of each batch of spheres in water was calculated using the Archimedes' method. This parameter is crucial in determining the amount of water required to saturate the spheres and the porosity of their shells.

The Archimedes density was determined by calculating the difference between the standard mass of the spheres (m) and their mass when submerged in water (m_s), using the following equation:

$$\rho_a = \frac{m}{m_s} \times \rho_w$$

where ρ_w represents the water density.

This method was performed with a density determination kit from METTLER TOLEDO. For a better understanding of the open and closed porosities present in the spheres' shells, these were also calculated, considering the density values obtained using the Archimedes' principle. Both porosities were calculated using the following equations:

$$Closed\ porosity\ (\%) = \left(\frac{\rho_m \times \rho_g - \rho_a \times \rho_g}{\rho_a \times\ \rho_m - \rho_a \times \rho_g}\right) \times 100$$

$$Open\ porosity\ (\%) = \left(\frac{\rho_a \times \rho_m - \rho_g \times \rho_m}{\rho_a \times\ \rho_m - \rho_a \times \rho_g}\right) \times 100$$

where ρ_m represents the theoretical density of hydroxyapatite (3.156 g.cm^{-3}) [54]. Moreover, the total porosity was also calculated through the equation:

$$Total\ porosity\ (\%) = \left(\frac{\rho_m - \rho_g}{\rho_m}\right) \times 100$$

3.2.2.3. Morphology and topography analysis

The porous spheres were further morphologically analyzed using scanning electron microscopy (SEM). This technique consists of replacing the light source with a high-energy electron beam, thus allowing the microstructure morphology to be observed [55].

For this purpose, a high-resolution (Schottky) environmental Scanning Electron Microscope with x-ray microanalysis and electron diffraction analysis: FEI Quanta 400 FEG ESEM / EDAX Genesis X4M was used. Furthermore, the samples were fractured in order to observe the core and were coated with a thin gold/palladium film for 20 seconds and with a 15 mA current by sputtering using SPI Module Sputter Coater equipment.

3.2.3. Drug release studies

Following the characterization of the spheres, the release of the two drugs, gentamicin, and alendronate, was assessed. The former being an antibiotic and the latter a bone resorption inhibitor.

The drugs were expected to be released from the delivery carriers in a controlled manner and maintain their effects for a considerable period [56].

The experiments were performed by varying the drugs concentrations. For each of those, 15 porous spheres were used, and each condition was performed in sextuplicate. All the conditions were tested using 1mL of release medium, which was deionized water in this case. The two drugs were also examined for their separate releases in addition to the dual-release studies.

3.2.3.1. Test samples

As previously stated, the release studies of alendronate and gentamicin were conducted both alone and combined for different concentrations of the two agents. Therefore, a total of four dual-release experiments were performed.

In two of them, the gentamicin concentration was varied while maintaining the alendronate one, and in the other two experiments, vice versa. In addition to these assays, the drug release was tested individually for each concentration administered, as it became apparent that it wasn't possible to quantify the drugs separately in the dual-release tests. The different release assays are detailed in table 2.

Table 2- Detailed conditions of the dual and individual release tests.

Samples	Sodium alginate solution (surface)	Gentamicin solution (surface)	Alendronate solution (core)
2G+1Al	2 % (w/v)	2 mg/mL	1 mg/mL
1G+1Al	2 % (w/v)	1 mg/mL	1 mg/mL
1G+3Al	2 % (w/v)	1mg/mL	3 mg/mL
1G+4Al	2 % (w/v)	1mg/mL	4 mg/mL
1G	2 % (w/v)	1 mg/mL	
2G	2 % (w/v)	2 mg/mL	
1Al	2 % (w/v)		1 mg/mL
3Al	2 % (w/v)		3 mg/mL
4Al	2 % (w/v)		4 mg/mL

All the solutions mentioned in this section were prepared in deionized water. All the gentamicin-alginate solutions have been prepared in a 50:50 volume ratio.

Initially, the release tests were performed with spheres loaded with the two drugs simultaneously, however, despite this being the main study of the project, it became apparent that it was not feasible to quantify the drugs separately. Gentamicin and alendronate are both detected by fluorescence spectroscopy at the same emission and excitation wavelengths and with the same reagent, leading to inaccurate results. Therefore, in order to be able to have an estimation of the drugs release profile, only the individual assays were quantified. However, the validation of the dual release tests was performed later through qualitative cellular and bacterial assays.

3.2.3.2. Drug loading in the spheres

In order to incorporate the two drugs in the spheres, 15 of these were placed in small flasks, with six replicates for each approach.

To all the flasks, 100 µL of alendronate aqueous solution were added at the required concentration for that assay (1 mg/mL, 3 mg/mL, or 4 mg/mL). The flasks were then covered with film, and a few small holes were poked into it so that vacuum could occur. They were then placed in a vacuum pump for 2 hours.

After two hours, any liquid remaining in the flasks was collected and stored for later analysis, in order to evaluate the efficiency of the drug loading.

Following this, 100 µL of a gentamicin-alginate solution at the intended concentration for that assay was added to each flask. The flasks were covered with film, and a few small holes were poked into it so that vacuum could occur. These were then placed in the vacuum pump overnight.

Any liquid remaining in the flasks was removed the following day and stored for later analysis, to evaluate the efficiency of the drug loading. Lastly, in order to crosslink the alginate-gentamicin solution on the surface of the spheres, 1 mL of a 10 % (w/v) $CaCl_2$ solution was added and left for 1 minute.

Figure 9 presents a schematic diagram of the spheres' loading process.

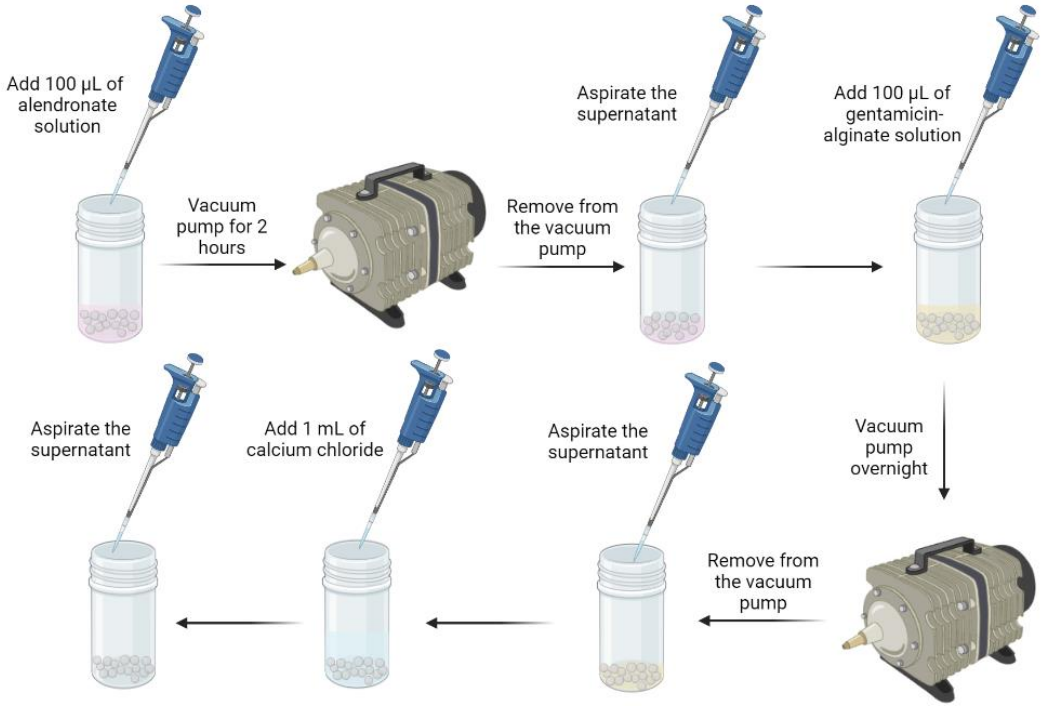


Figure 9- Loading process of the two drugs in the spheres. Created with BioRender.com.

Regarding the drug incorporation for the individual release assays, the same methods were used. However, only the desired drug was loaded.

Concerning the gentamicin adsorption on the sphere, 100 µL of the alginate-gentamicin solution was added to all the flasks, and these were placed in the vacuum pump overnight. The following day, crosslinking with the calcium chloride solution was performed in the same way as in the dual release assays.

As for the incorporation of alendronate in the spheres, 100 µL of alendronate solution was added to all the flasks. These were then placed in the vacuum pump and left for 2 hours. After this period, any liquid that remained in the flasks was removed, and 100 µL of 2 % (w/v) alginate solution was added. The flasks were placed in the vacuum pump again and left overnight. The crosslinking process followed the same procedure as described above.

3.2.3.3. Release profiles

Once the spheres were loaded, 1 mL of release medium (deionized water) was added to each flask, and these were placed in an orbital shaker (IKA® KS 4000 ic control) at a temperature of 31 ºC at 60 rpm. The release of the 15 spheres was registered at the following time points: 2, 4, 6, 8, 24, 48 hours, and every 24 hours thereafter. At each time point, 50 % of the supernatant volume (500 µL) was collected and replaced with deionized water.

After collecting the supernatant, this was stored in labeled 48-well plates. Lastly, these were placed in the refrigerator for later analysis.

3.2.3.4. Gentamicin spectrophotometric quantification

The amount of gentamicin loaded into each batch of spheres was quantified by analyzing the supernatant that remained in the flask after each vacuum cycle. This quantification was performed by fluorescence spectrophotometry, using the same approach that was used for the release tests described below.

For this purpose, 65 µL of the supernatant were collected and analyzed at an excitation wavelength of 360 nm and emission of 460 nm. The control was subtracted from each absorbance value obtained, and thus the gentamicin concentration was determined. The drug loading efficiency was estimated using the following equation:

$$Loading\ efficiency\ (\%) = \frac{gentamicin\ mass\ added\ initially - gentamicin\ mass\ in\ the\ supernatant}{gentamicin\ mass\ added\ initially} \times 100$$

The concentration of gentamicin released at each time point was also determined using fluorescence spectrophotometry. 65 µL of the previously saved supernatant from each sample were collected into a black 96-well microplate suitable for fluorescence spectrophotometry. A

calibration curve was prepared using gentamicin concentrations between 0 µg/mL and 1000 µg/mL. 65 µL of each solution made to prepare the calibration curve were also pipetted to the plate. To each of these wells 75 µL of methanol and subsequently, 115 µL of a solution containing o-Phthalaldehyde (OPA) reagent and methanol in a 1:8 volume ratio were also added. The o-Phthaldialdehyde reagent (OPA) was formulated by adding 0.2 g of o-phthaldialdehyde to 1 mL of methanol. To this solution, 15 mL of borate buffer and 0.4 mL of 2-mercaptoethanol were added. Finally, the pH was adjusted to 10.4 with potassium hydroxide. Fluorescence was then measured in a microplate reader (Synergy HT, Biotek).

3.2.3.5. Alendronate spectrophotometric quantification

Similar to what was described in the previous section (3.2.3.4), the spectrophotometric quantification of alendronate was performed via fluorescence spectrophotometry in a microplate reader (Synergy HT, Biotek), using the exact same strategy as was used for the quantification of gentamicin.

A calibration curve was prepared using alendronate concentrations ranging from 0 µg/mL to 1000 µg/mL. The amount of alendronate released at each time point is determined using the same reagents in the exact same amounts that were used for the quantification of gentamicin at the same wavelength. The alendronate concentration was determined after subtracting the control from each absorbance value obtained.

Loading efficiency was also calculated for each assay by quantifying via fluorescence spectrophotometry the supernatant remaining in each vial after each vacuum cycle. The loading efficiency was estimated using the equation:

$$Loading\ efficiency\ (\%) = \frac{alendronate\ mass\ added\ initially - alendronate\ mass\ in\ the\ supernatant}{alendronate\ mass\ added\ initially} \times 100$$

3.2.4. Antimicrobial activity assessment

To assess the antimicrobial activity of the spheres, the agar diffusion test was performed. For this purpose, spheres under different conditions were placed directly on inoculated *Mueller Hinton* agar medium. As such, spheres from the conditions 1Al, 2G+1Al, 1G+1Al, 1G+3Al, and 1G+4Al, which are detailed in section 3.2.3.1 in table 2, as well as non-loaded spheres, were used.

Five spheres were used for each day of this experiment and for each loading condition, as can be observed in figure 10.

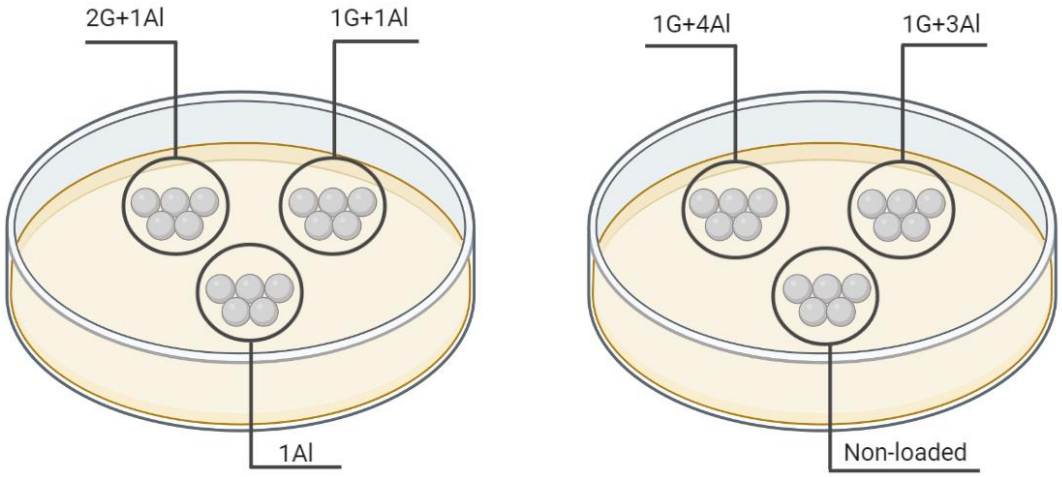


Figure 10- Placement representation of the spheres in the Petri dishes. Created with BioRender.com.

3.2.4.1. Culture medium preparation

The *Mueller Hinton* agar medium was prepared by dissolving 38 g of powdered medium in one liter of deionized water. It was then placed on a hot plate magnetic stirrer in order to achieve complete dissolution. Afterward, the medium was sterilized through autoclaving at 121 ºC for 15 minutes.

Near the Bunsen burner, in sterile conditions, the medium was distributed among the Petri dishes. These were left to cool at room temperature and then placed in the refrigerator overnight.

3.2.4.2. Bacterial suspension preparation

The bacterial strain *Staphylococcus aureus* ATCC 29213 was used in this experimental activity.

Firstly, the absorbance of a saline solution (NaCl 0.9 %) was measured at 640 nm in the spectrophotometer to zero the device. A volume of about 5 mL of this solution was dispensed into a falcon, and a few colonies of the strain were subsequently collected and placed in the same falcon using an inoculating loop.

Afterward, the falcon was vortexed to achieve a homogeneous bacterial suspension. The turbidity of this suspension was subsequently analyzed using the spectrophotometer, at 640 nm. The absorbance should be comprised between 0.10 and 0.15, which corresponds to 10^8 CFU/mL within the suspension.

However, it is necessary to adjust the suspension if its absorbance is not between these values. Such adjustment is done by adding more saline solution (if abs > 0.15) or more bacterial colonies (if abs < 0.10).

3.2.4.3. Mueller Hinton agar diffusion test

To mimic what occurs in the release tests, 75 spheres of each condition were placed in flasks with 5 ml of distilled water, a proportional volume to that used in the release experiments. The flasks were then placed in an orbital shaker oven (IKA® KS 4000 ic control).

The previously prepared Mueller Hinton medium was then inoculated with the bacterial suspension using a swab. Three spreads over the entire surface of the agar plate were made while rotating it to ensure an even distribution of the bacteria.

Every 24 hours up to seven days, 5 spheres were collected and placed in the inoculated Petri dishes in order to evaluate the inhibition halo. 50 % of the release medium was removed and replaced with distilled water, adjusting the volume every time spheres were removed.

3.2.5. In vitro *biological evaluation*

In all the experiments performed from this point forward, lyophilized and ethylene oxide sterilized spheres were used. The spheres were sterilized at the São João Hospital Center at 50 ºC and left to aerate for two days. Cells of the MG-63 lineage were used to assess the cytotoxicity of loaded and non-loaded spheres as well as alendronate by itself.

For this purpose, spheres from the conditions 1G+1Al, 1G+4Al, and 2G+1Al, described in section 3.2.3.1, as well as non-loaded spheres were used. Furthermore, to evaluate the cytotoxicity of the compound itself, alendronate solutions at concentrations of 10^{-4} M, 10^{-5} M, 10^{-6} M, and 10^{-7} M were tested. The choice for this concentration range emerged from the fact that several articles reported that alendronate concentrations between 10^{-5} M and 10^{-11} M promoted MG-63 cell proliferation, while 10^{-4} M concentrations of the same compound inhibited it [57].

3.2.5.1. Cytotoxicity evaluation of the samples

MG-63 cells were cultured in alpha-Minimum Essential Medium (α-MEM) supplemented with 10 % (v/v) fetal bovine serum and 1 % (v/v) of a solution containing 10000 U/mL of penicillin, 10000 µg/mL of streptomycin, and 25 µg/mL of amphotericin B (complete α-MEM).

In this experiment, the cells were seeded in 96-well plates at a density of 2×10^4 cells/cm^2 with 10 spheres per well. These were further incubated up to 10 days at 37 ºC, in a 5 % CO_2 humidified atmosphere. To better comprehend, the positioning of the spheres in the 96-well plate is schematically shown in figure 11.

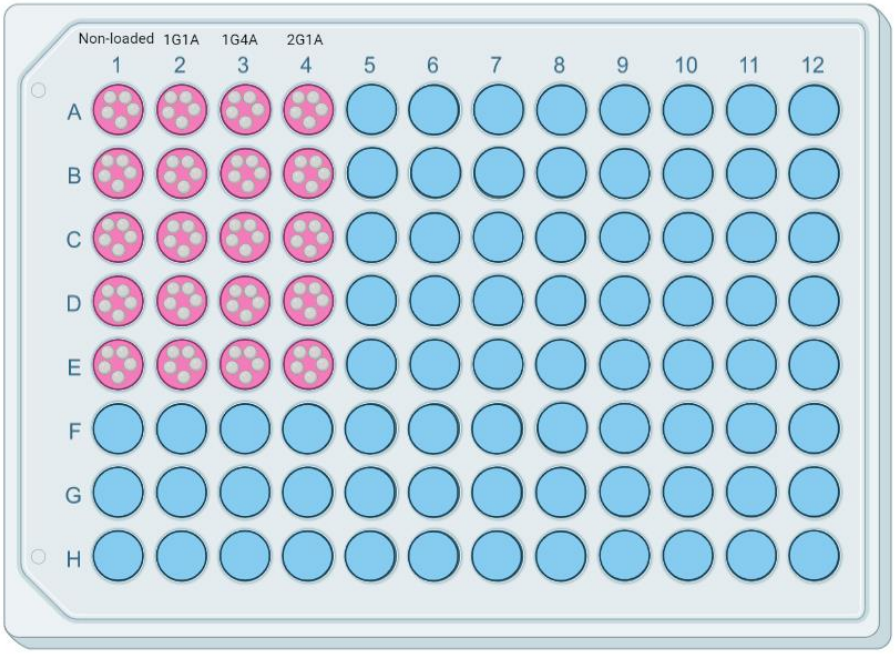


Figure 11- Layout representing the placement of the spheres in the 96-well plate. Created with BioRender.com.

3.2.5.2. Cytotoxicity evaluation of the compound

To assess the cytotoxicity of different concentrations of alendronate, cells were seeded at $1x10^4$ cells/cm^2 in a 96-well surface treated plate in complete α-MEM for 24 hours, under the same incubation conditions as described above. After this period, these were further exposed to the diluted compound in medium at various concentrations (10^{-4} M, 10^{-5} M, 10^{-6} M, and 10^{-7} M). Additionally, a control group was also performed, where the spheres were only exposed to the complete α-MEM culture medium.

3.2.5.3. Resazurin assay

The cellular metabolism was evaluated using the resazurin assay. At each time point, the medium was removed from the wells and replaced with culture medium containing 1 % (w/v) resazurin (0.1 mg/mL). The plates were incubated for 2 hours at 37 °C.

After this period, fluorescence was measured (excitation: 530 nm; emission: 590 nm) in a microplate reader (Synergy HT, Biotek).

3.2.5.4. Cell morphology analysis

To examine the morphology of the MG-63 cells adhered onto the spheres, a SEM analysis was performed. The samples were washed with PBS and fixed with 100 µL of a 1.5 % (v/v)

solution of glutaraldehyde in sodium cacodylate buffer (pH 7.3) for 20 min. After this period, these were again washed with PBS and 100 µL of sodium cacodylate buffer were added.

Subsequently, the samples were dehydrated using ethanol solutions ranging from 50 % (v/v) to 100 % (v/v), and critical point dried (CPD 7501, Polaron Range). Finally, the samples were sputter-coated (SPI-Module) with a gold/palladium thin film and visualized, in the same conditions as described above.

3.2.6. Statistical analysis

The statistical analysis of the data was performed using the *t-test* with a significance level of $p<0.05$. The number of independent runs for each experiment (N) is indicated in the caption of the respective figure. The data are presented as mean±standard deviation.

Chapter 4: Results and Discussion

4.1. Production and characterization of the porous spheres

4.1.1. Production of the hollow spheres

As previously mentioned, the syringe-foaming method was employed to obtain the porous ceramic spheres, using a ceramic suspension, composed of alginate and hydroxyapatite, and a surfactant, Pluronic F-127. Together with the ceramic suspension, the surfactant was used to form a ceramic foam that imparted the desired porosity onto the ceramic spheres, thus being a key element in this system. Pluronic F-127 has been extensively studied for the sustained delivery of pharmaceutical agents, which makes it suitable for this study [58].

Pore interconnectivity is also extremely relevant in this context, because, apart from conferring a greater diffusion of nutrients to deeper areas and allowing vascular invasion, it has a great influence on drug delivery systems [2], [59]. The interconnective porosity of a bone regeneration material is a crucial feature since this property will allow the formation of new bone tissue as well as its vascularization and an accurate diffusion of nutrients throughout the scaffold by facilitating cellular attachment and proliferation [22]. Furthermore, it has also been shown that scaffold porosity and pore interconnectivity have a major impact on the material's resorption rate such that introducing interconnective pores into the scaffold enhances its integration with the host tissue and new vessels ingrowth from existing ones, resulting in an increased resorption rate [60], [61]. The produced spheres were expected to have great pore interconnectivity, in order to favor their drug loading as well as controlled drug release.

In this system, alginate was the agent responsible for conferring the spherical shape to the ceramic foam upon contact with the crosslinking agent, the calcium ion (Ca^{2+}) present in the $CaCl_2$ solution, which resulted in the alginate gelation. Furthermore, the sunflower oil was employed in this system since it is hydrophobic and immiscible with the ceramic foam. Thus, there was a phase separation between the ceramic foam and the oil, whereas, after the heat treatment, this oil was combusted, leaving a hollow core inside the sphere. When producing the hollow spheres, acetone was responsible for dehydrating them. This dehydration was essential to achieve better control in the heat treatment process. If the spheres were not dehydrated prior to heat treatment, their shrinkage rate would be higher than desired.

4.1.2. Heat treatment

Initially, in this heat treatment cycle, the organic compounds, such as the Pluronic F-127 and the sunflower oil were combusted, which accounted for the formation of the pores and the hollow core within the spheres, respectively. Only during the last phase of the process, the hydroxyapatite was sintered.

The sintering method employed in this process was solid-state sintering. Here there was the densification of the hydroxyapatite particle aggregate in the sphere, involving its contraction, with the application of high temperatures below the material's melting point [53]. Thus, after the heat treatment, the spheres shrank, and their pore size reduced. Additionally, as part of other work carried out by the research group, an X-ray Powder Diffraction (XRD) analysis was performed, which demonstrated that pure phase hydroxyapatite was obtained after sintering.

4.1.3. Morphological observation under the stereomicroscope

As a quality control measure for each batch of spheres produced, these were observed under the stereomicroscope after the sintering process. This method was used to verify the uniformity and quality of the produced spheres by observing the homogeneity of their surfaces and the co-injection efficiency and consistency through the sphere core's centricity.

Based on figure 12A, it was possible to observe the uniform surface of the sphere. By observing figure 12B, where the sphere's core is represented, it was possible to infer that the core was centered, which confirms the efficiency of the co-injection process. Some porosity was also visible in the sphere. However, in the SEM analysis, this was more perceptible.

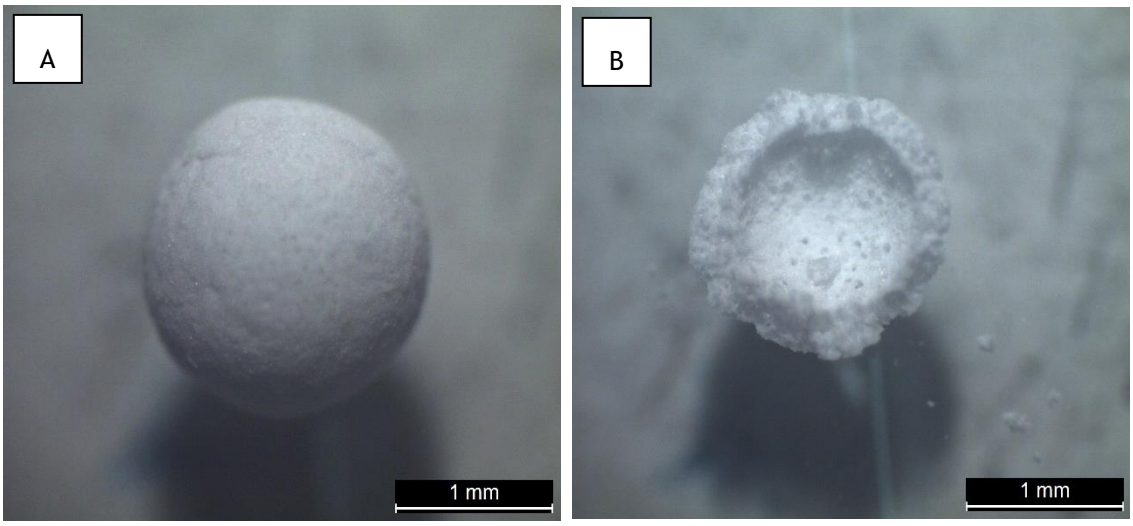


Figure 12- Representative stereomicroscope images of the surface (A) and the core (B) of the hydroxyapatite hollow spheres.

4.1.4. Morphology and topography analysis

The examination using SEM was essential for observing the porosity and the interconnected network present in the ceramic spheres, as well their shape, size, the centricity of their cores, and the thickness of their shells. Ideally, the spheres should have a porous structure and an interconnected pore network, since, as previously stated, these properties will promote bone ingrowth upon scaffold implantation [2]. Furthermore, a scaffold's pore size also impacts cell differentiation and adhesion and hence bone ingrowth.

When analyzing figure 13A, obtained by the SEM technique, it was apparent that the pore sizes range from 75 µm to 106 µm. The obtained values are suitable for the intended application as they are in agreement with previous studies, where it has been shown that the minimum pore size for significant bone growth post-implantation is between 75 µm and 100 µm [62]. It was still possible to observe the pore interconnectivity which will be further verified by the results obtained in section 4.1.5. By analyzing figure 13B, it was evident the intercommunication between the pores within the shell and the hollow core of the spheres and it was also noticeable the presence of pores on the surface that had direct communication with the ones on the inside of the sphere. This will obviously favor the spheres' loading with the alendronate and gentamicin since it increases the drugs' uptake capacity. This interconnectivity associated with the pore size obtained will be important in providing a high surface area to the spheres, which promotes cell adhesion and will enhance the sphere's capacity to incorporate drugs. Concerning these criteria, it is possible to state that the spheres have ideal characteristics for bone ingrowth. Additionally, it was notable the concentricity of the spheres' core and the integrity of their shells, once again. However, since not all the samples were examined through this technique it was not possible to assume that all the spheres used in the subsequent experiments have the same properties.

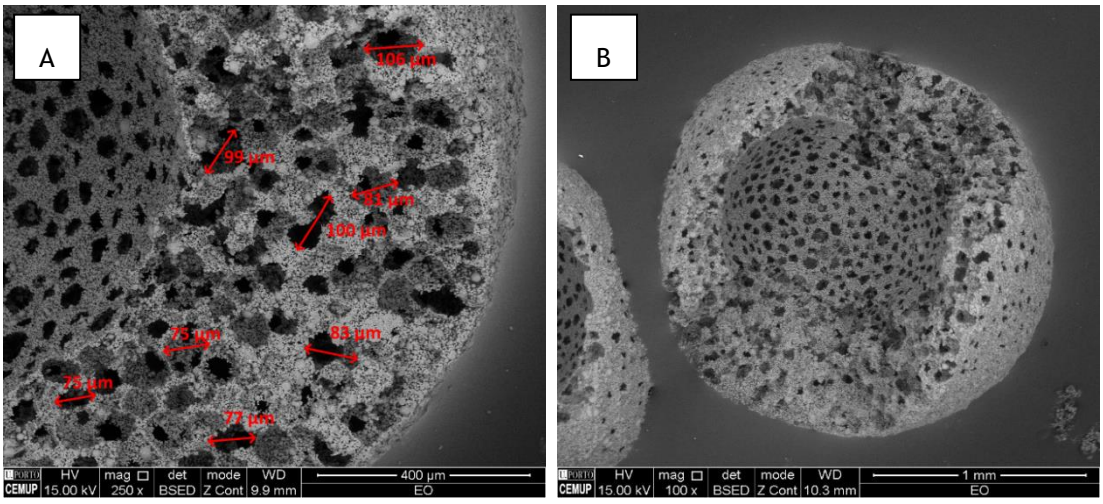


Figure 13- Representative SEM images of a hollow porous sphere post-sintering at 250x magnification, highlighting its pores and respective diameters measured in ImageJ software (A) and at 100x magnification highlighting the sphere's core and surface (B).

4.1.5. Porosity analysis

Archimedes' principle is frequently employed in measuring the density of an irregular material [63]. Therefore, it was the selected method for measuring the density of the hollow spheres, following the heat treatment.

After measuring the masses and the diameters of the spheres for each batch, the spheres' volumes were also inferred. To obtain the most realistic porosity values, it was necessary to subtract the value of the core volume from the theoretical volume of the spheres, as described in section 3.2.2.2. The reason for this strategy is that if the core of the spheres were taken into account for the calculations, it would be considered a large pore, making it difficult to obtain the porosity results only for the pores in the sphere's shell and the values obtained would not be accurate. Furthermore, since the samples used were broken in half, the Archimedes density obtained using this method only reflected the one in the spheres' shell. The volume of the spheres' core was deduced from SEM images, as can be seen in the figure 14, the core diameter is 1.006 mm, which corresponds to a volume of 0.533 mm^3. Based on the geometric and Arquimedes densities obtained by this method it was then possible to determine the open and closed porosity of the spheres' shells, using the equations outlined in section 3.2.2.2.

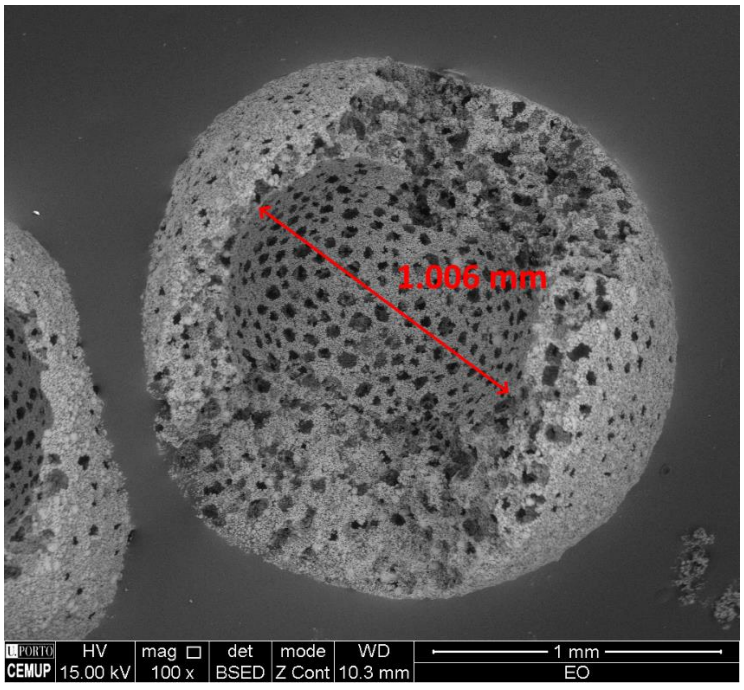


Figure 14- Representative SEM image of the hollow sphere after sintering at 100x magnification and the respective core diameter measured in ImageJ software.

The average total porosity obtained for the spheres' shells was 64.89±1.47 %. Out of these, 57.51±4.11 % corresponded to open porosity and 42.49±4.11 % to closed porosity. The acquired data may thus be used to deduce that the spheres' shells had a more significant

amount of open pores than closed ones. This translated into a greater interconnectivity within the spheres' shell, as there were more pores that communicated with the exterior versus closed pores, as expected.

As previously mentioned, the pore interconnectivity is a crucial factor in this system since this property of the spheres will be responsible for the controlled release of the drugs rather than a burst release [59], as well as the effective drug-loading into the spheres. As most of the pores present in the spheres' shells were in contact with each other by forming ducts, it was expected that the drugs were released in a phased pattern over time. Furthermore, under the perspective of tissue engineering and bone regeneration, the porosity and interconnectivity of the pores can have a favorable influence on the recruitment of cells as well as their adhesion to the material when implanted, while also facilitating the invasion of blood vessels from surrounding tissues and allowing the passage of fluids and nutrients, when implanted [2], [23]. The total porosities of the sphere shells obtained also meet the trabecular bone porosity values described in the literature (55-70 %) [64].

4.2. Drug release studies

In order to trace the release profiles of the two incorporated agents, release studies were performed. As previously explained in section 3.2.3.1, through fluorescence spectrophotometry, it was not possible to separate the release profiles of the two drugs, which would be ideal. The only alternative for quantifying the release of the two drugs in the dual-release assays would be to use the high-performance liquid chromatography (HPLC) method which would not be viable in this context. Therefore, only the individual release assays were considered for these experiments.

Since most of the gentamicin was expected to be adsorbed onto the sphere's surface as well as within the alginate mesh, and conversely, most of the alendronate was to be allocated on the sphere's core and in their interconnective pores, it was anticipated that the release patterns would differ. Thus, gentamicin was predicted to be released faster than alendronate, which was intended to have a release during a more extended period.

4.2.1. Drug loading

A factor that will influence the performance of this dual release system is the loading efficacy of the two agents in the spheres. Using the equations presented in sections 3.2.3.4 and 3.2.3.5 it was possible to calculate the loading efficiency, considering the mass of gentamicin and alendronate incorporated in 15 spheres for each condition. Analyzing table 3, it was possible to observe that in the two gentamicin conditions, 1G and 2G, the loading efficiencies were 60.56±0.39 % and 53.69±0.10 %, respectively. Furthermore, in the 3

alendronate conditions, the loading efficiencies for the 1Al, 3Al, and 4Al tests were 75.65±0.85 %, 91.53±0.16 %, and 89.61±0.24 %, respectively. This reflected a successful loading of the porous spheres. Additionally, it is worth bearing in mind that the administered solution volume of both alendronate and gentamicin in each vial was 0.100 mL, which resulted in a theoretical loaded volume of 0.0067 mL (6.7 mm^3).

As previously stated, it was possible to infer that the core volume of the spheres was around 0.533 mm^3. Therefore, the volume of alendronate administered to each sphere was greater than their core capacity, which reflected the presence of alendronate in the sphere's shell pores and not only in its core. This was also corroborated by the great pore interconnectivity present in the spheres. However, even if the capacity of the sphere's core was sufficient for the total absorption of the alendronate volume administered, there would always be traces of the compound in the pores of the sphere where it penetrated.

*Table 3- Loading efficiency of the gentamicin (1G, 2G) and alendronate (1Al, 3Al, 4Al) conditions, determined by fluorescence spectrophotometry. *=p<0.05 between conditions 1G and 2G, for N=6. ¨=p<0.05 among conditions 1Al, 3Al and 4Al, for N=6.*

Test condition	*Loading efficiency (%)*
1G	60.56 ± 0.39 *
2G	53.69 ± 0.10 *
1Al	75.65 ± 0.85 ¨
3Al	91.53 ± 0.16 ¨
4Al	89.61 ± 0.24 ¨

4.2.2. Gentamicin release studies

In dentistry and orthopedics, bacterial adhesion and the resulting biofilm development constitute a significant issue since the consequent infection could result in implant failure, long hospitalization, several surgical interventions, and worst-case scenario, limb amputation. Surgical-site infection is a phenomenon that develops in the region where the procedure was done. It may be quite superficial, affecting the skin only. However, sometimes it can be more serious, affecting skin, tissues, organs, or even implanted materials [65], [66]. Surgical-site infections are a global occurrence. In the United States alone, the annual prevalence of these infections is estimated to be 1.07 %, with 8000 fatalities directly linked to these infections and a treatment cost of up to $10 billion. In addition, the European Center for Disease Control has estimated that 3.7 million people acquire a healthcare-associated infection each year in hospitals in European union countries as well as in Norway and Iceland [67], [68]. Bacteria of the *Staphylococcus* genus comprise a large proportion of the pathogens involved in these infections. The ability of these organisms to form small colonies and grow in biofilms makes

these infections challenging to manage [69]. High concentrations of antibiotics are commonly administered orally to reach effective concentrations at the infected site, which turns out not to be the best approach as it can lead to the development of resistant bacteria, as well as cellular toxicity and side effects on the bone regeneration process. Loading the scaffolds with antibiotics in order to have a local release, is a prospective technique for tissue regeneration to enhance the healing of the injured bone tissue and to overcome this problem [44], [70].

For the present investigation, gentamicin was the antibiotic employed since it has a broad spectrum of activity against gram-positive and gram-negative bacterial species [41]. To have an actual antibacterial action, gentamicin must be released from the spheres at doses that are higher than the minimum inhibitory concentration (MIC) for the pathogen in question, in this case, *Staphylococcus aureus (S. aureus),* a gram-positive representative bacterium.

S. aureus is a pathogenic agent of clinical importance due to its prevalence in causing nosocomial and surgical site infections in addition to being the most common pathogenic bacterium responsible for bone infections. These bacteria may lead to acute bone loss and destruction after infection. This happens because, upon infection with *S. aureus*, osteoblasts weaken and begin to suffer necrosis and apoptosis. Simultaneously, osteoclast proliferation and bone metabolic balance are disturbed, causing inflammatory bone loss [71], [72]. Therefore, the values obtained in the gentamicin release profiles were compared to those reported in the literature on minimum inhibitory concentration for *S. aureus*, due to its prevalence in clinical settings and thus it is important that the spheres have an inhibitory effect for this pathogen. Previous studies have reported that the MIC for the strain used in this study (MSSA ATCC 29213) is 1 µg/mL, while the MIC of the clinical strains (MRSA 8111) is around 2 µg/mL [73].

4.2.2.1. Gentamicin release profiles

As previously mentioned, a gentamicin-alginate solution was used for the loading of the spheres. Alginate is a biocompatible polysaccharide polymer consisting of D-mannuronic acid and L-glucuronic acid. It is capable of forming fairly stable hydrogels via ionotropic gelation in the presence of cations such as Ca^{2+}. It has become extensively used as a drug carrier due to its biodegradability, low immunogenicity, commercial availability, and affordability. The combination of drug carriers such as alginate with a sustained antibiotic release can have a beneficial effect in decreasing the systemic toxicity and side effects of antibiotics. A reported study demonstrated that the presence of alginate in drug delivery systems significantly reduced the initial burst release of gentamicin and consequently provided a sustained release of the drug, for concentrations of 2.5 and 5 %/w, over a more extended period [74]. Combining the sustained antibiotic release with the osteoconductive and resorbable properties of the porous hydroxyapatite spheres will provide a double beneficial effect. The scaffold will provide specific treatment for the infection while stimulating bone regeneration [75].

Figure 15 displays the gentamicin release profiles for both test conditions (1G and 2G), as well as the cumulative mass percentage graphs. Overall, by looking at the charts, it can be stated that for both test conditions, the release profile was quite similar. At the initial time point (2 hours), a release peak was evident, followed by a decline in the concentration of released gentamicin until it stabilized around days 2-3. By these time points, approximately 55 % and 42 % of the mass of gentamicin incorporated was released in assays 1G and 2G, respectively. The initial burst release at the early time points is a major contributor to the antibacterial efficacy of the porous spheres, as it provides a high concentration of antibiotic that is required in the critical period immediately after surgery, where there is more susceptibility to develop an infection. On the other hand, the sustained release provides a continuous dosage of the antibiotic for long-term treatment [75].

When comparing the two conditions' charts, it can be noted that within the first 6 hours of the experiment, the concentration of released gentamicin was considerably higher in condition 2G than in 1G. This was expected, since the concentration of the solution administered to the porous spheres in the 2G assay was twice as high as in the 1G, as described in section 3.2.3.1. However, after the initial 6 hours, the released gentamicin concentration was quite similar for both samples. It can also be noted from analyzing the charts in figure 15 that for conditions 1G and 2G the release profiles exhibited a plateau starting on day 3 and 2, respectively. This plateau remained up to day 16 in both experiments, meaning that for 13 and 14 days the spheres were releasing similar daily concentrations of gentamicin for the 1G and 2G conditions, respectively. This demonstrated the controlled and sustained release of the embedded drug from the porous spheres. Such controlled release is due to the presence of alginate; previous investigations have found that gentamicin sulfate selectively reacts with mannuronic residues present in alginate, and, thus, gentamicin molecules will become incorporated into the network of this hydrogel. Moreover, this sustained gentamicin delivery occurred because a highly viscous hydrocolloidal layer was formed after the alginate had been hydrated. This layer provided a diffusion barrier, slowing the migration of small molecules such as drugs. Therefore, the gentamicin concentration gradient was the driving force for the diffusion of this compound from the spheres onto the release medium [76].

From the cumulative mass percentage plots (figure 15b), it was possible to state that condition 1G performed better compared to the 2G. Since, by day 27, approximately 81 % of the gentamicin incorporated in the spheres had been released, whereas, in condition 2G, only 59 % had been released after the same period. It is worth considering that the desired time for the complete release of gentamicin in this project was around 15 days. Therefore, although the release profiles of both gentamicin experiments were quite similar, it was possible to note that after 15 days, condition 1G had the highest amount of released gentamicin compared to 2G. Consequently, condition 1G proved to be more successful since it presented a more suitable release kinetics for the intended application.

Furthermore, when comparing the graphs with the reported value in the literature of minimum inhibitory concentration for *S. aureus* bacteria (MIC from 1 µg/mL to 2 µg/mL) it was possible to observe that as long as there was gentamicin release, the concentration released was always above the MICs for both conditions tested. These outcomes will be further evaluated in the bacterial experiments.

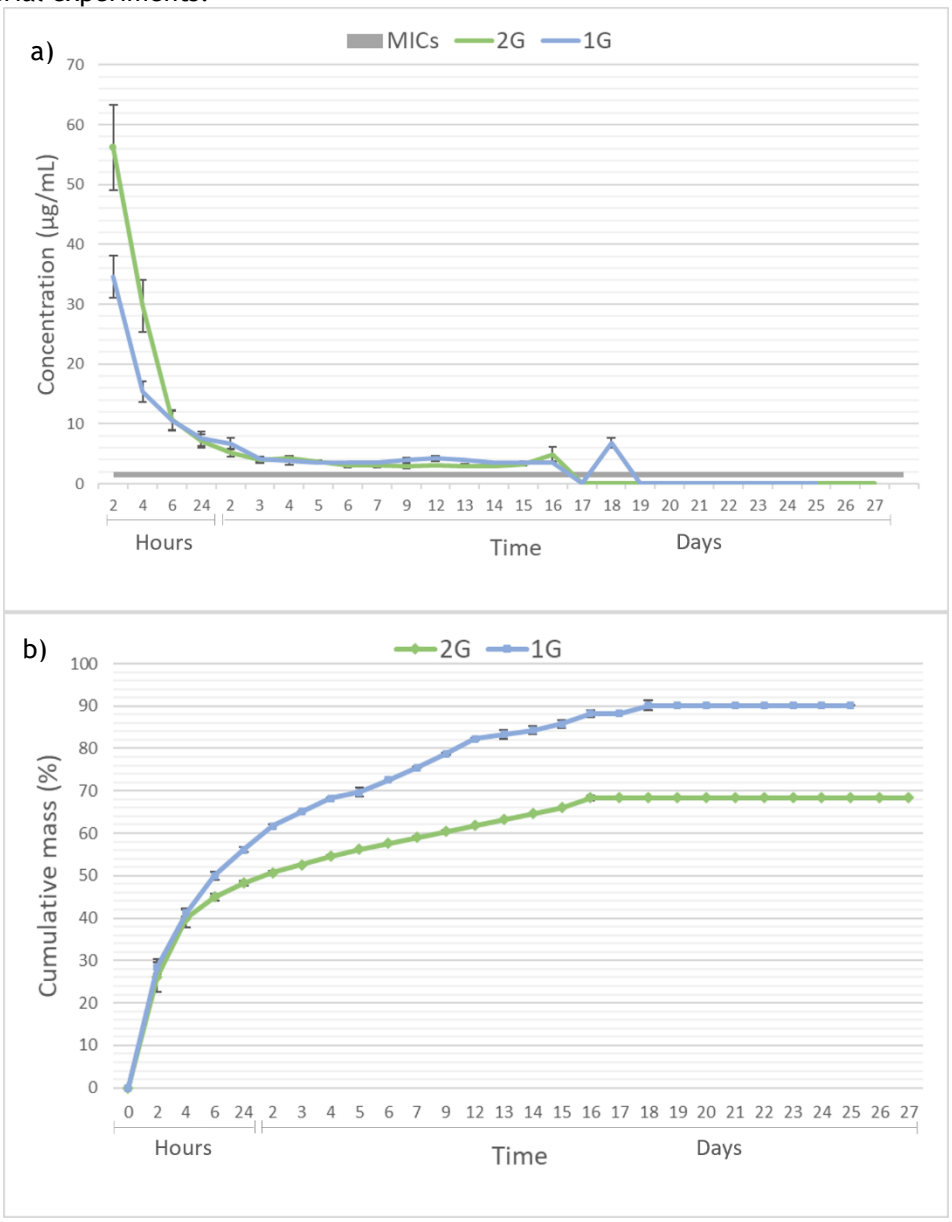


Figure 15- Gentamicin concentration release profile (a) and cumulative mass percentage of gentamicin released (b) in the 1G and 2G conditions over 28 days.

4.2.3. Alendronate release studies

Osteoporosis has been recognized as the leading cause of bone fractures worldwide and the most diagnosed bone disorder. Studies have shown that over 200 million people globally suffer from this disease. Annually, osteoporosis is accountable for more than 8.9 million cases of fracture. Bisphosphonates such as alendronate are the most often used therapeutic

medicines for treating diseases characterized by increased osteoclastic activity and enhanced bone resorption. Furthermore, bisphosphonates have also been found to be effective in enhancing bone mineral density in cases of osteopenia, a disease that results in loss of bone density and may ultimately lead to osteoporosis [77]. These agents can disrupt the osteoclasts' cytoskeleton, leading to their death, thus reducing the loss of bone mass. Nevertheless, despite their medicinal effectiveness, they have some drawbacks, such as limited oral bioavailability (1 %-3 %), side effects of acute gastrointestinal disorders, and others. Improvements in the design of drug delivery systems are one attempt that has been made to increase the bioavailability of bisphosphonates while reducing the associated side effects as well. These drugs have an outstanding attraction to bone hydroxyapatite, which results in bisphosphonates deposition in the proximity of osteoclasts in newly formed bone. During the resorption phase, the osteoclast microenvironment becomes acidic, which may promote the release of bisphosphonates from the bone surface. As a result, this agent's local concentration is increased on the bone mineral surface, especially at the site of osteoclast activity, through a rapid release from the systemic circulation [36]. Previous studies have reported that alendronate has a concentration-dependent effect on osteoblast-like cells, increasing the proliferation of primary human trabecular bone cells and MG-63 cells (human osteosarcoma cells) over a 10^{-5} to 10^{-11} M concentration range. On the other hand, the proliferation of these cells was also shown to be inhibited at 10^{-4} M alendronate, which is believed to be due to the cytotoxicity of the compound at this concentration. Alendronate is also believed to have the greatest effect on these cells at a concentration of 10^{-8} M [57]. Additionally, alendronate concentrations between 10^{-5} M and 10^{-7} M have been demonstrated to significantly inhibit bone resorption [78].

4.2.3.1. Alendronate release profiles

In comparison to the existing variety of bisphosphonates, alendronate has a medium potency, which is suitable for a preliminary investigation and was therefore the agent chosen for this study. In figure 16, it is possible to observe the alendronate release profile for the three conditions tested (1Al, 3Al and 4Al) and the cumulative mass percentage of alendronate released throughout each test.

For the 1Al condition, it was evident by analyzing the release profile and cumulative mass percentage plots that the alendronate release exhibited a pulsatile pattern. It was possible to observe through the charts that there were release peaks at the initial time points, and in the 3 to 21 days interval, there was no release of alendronate, followed by release peaks on the experiment's final days. From the cumulative mass percentage plot, it is also possible to infer that approximately 52 % of the encapsulated alendronate had been released after 3 days of the experiment. From this time-point until 21 days, the plot exhibited a plateau,

confirming that there was no release in this period. After this time, the remaining amount of alendronate was released until the end of the experiment (27 days).

By analyzing the 3AL condition plot, it was also possible to recognize a pulsatile pattern, where there was a release of alendronate until the fourth experiment day, followed by a period of 11 days where there was no release. From day 16 to 24, there was a relatively constant alendronate clearance, and on the experiment's final days, there was no release. Through the cumulative mass percentage graph, it was possible to confirm this pulsative pattern of the release kinetics and its sustained release since only at the end of 16 days, 54 % of the encapsulated alendronate had been released.

Finally, by analyzing the graphs for condition 4Al, it can also be noted that its release pattern, while more constant than in the other two conditions, exhibited a relatively pulsatile behavior. It also exhibited a controlled release behavior, as shown in the cumulative mass percentage graph, where only by day 12, 52 % of the encapsulated amount of alendronate was released. This plot displayed a linear behavior up to the 23rd day of the experiment, which confirms the steadier release compared to the other two conditions. It should also be noted that until day 23, there were no periods without drug release.

As discussed in section 4.2.1, there is the presence of alendronate in the spheres' shell pores and not only in their cores. This is because the drug was adsorbed along the pores within the spheres' shell, during the alendronate loading process. Therefore, since not all the encapsulated alendronate was stored in the sphere's nucleus, there were variations in the release times of this drug. Evidently, the alendronate molecules confined in the pores nearest the sphere's surface were released first, corresponding to the first release peak, and so on. Therefore, there was a release throughout the layers of pores present in the sphere's shell resulting in a pulsatile pattern. Within the context of this work, having a drug release with a pulsatile pattern is a positive aspect since, according to reported studies in the literature, a pulsatile release, significantly promotes osteogenic differentiation, via stimuli, for the treatment of bone conditions such as osteoporosis [79]. When comparing the individual release patterns of the three conditions tested, it can be stated that the 1Al condition had the highest therapeutic potential since it was the one that had a more pulsatile profile, promoting a more significant osteogenic differentiation.

By observing the release patterns of the three conditions, it can be noted that the higher the administered concentration of alendronate, the closer to stability the release pattern was. This phenomenon is consistent with previous studies on controlled diffusion of drugs that report that as long as the saturation of a compound in the hydrogel is maintained, there will be a stationary concentration gradient across the diffusion membrane, and the release will proceed at a constant rate [80]. Therefore, in the 4Al assay, it is likely that alendronate saturation in the alginate was maintained for a more extended period. Thus, there

was a steadier release than in the other two conditions, hence the difference between the three release profiles.

In the present study, the time frame for the alendronate release was around 24 to 28 days. Considering the spheres' purpose, this is a suitable release period for this drug, as literature studies suggest that scaffolds containing alendronate have a twofold effect of enhancing osteoblast differentiation and inhibiting osteoclast differentiation simultaneously over a period of 21 days [81]. Among all the alendronate release experiments described, the release concentration lied within the range of 10^{-5} M to 10^{-4} M, which, as mentioned earlier, according to the literature encountered, are in the cytotoxicity threshold for osteoblast-like cells [57]. This cytotoxicity evaluation will be performed later, in the cellular tests.

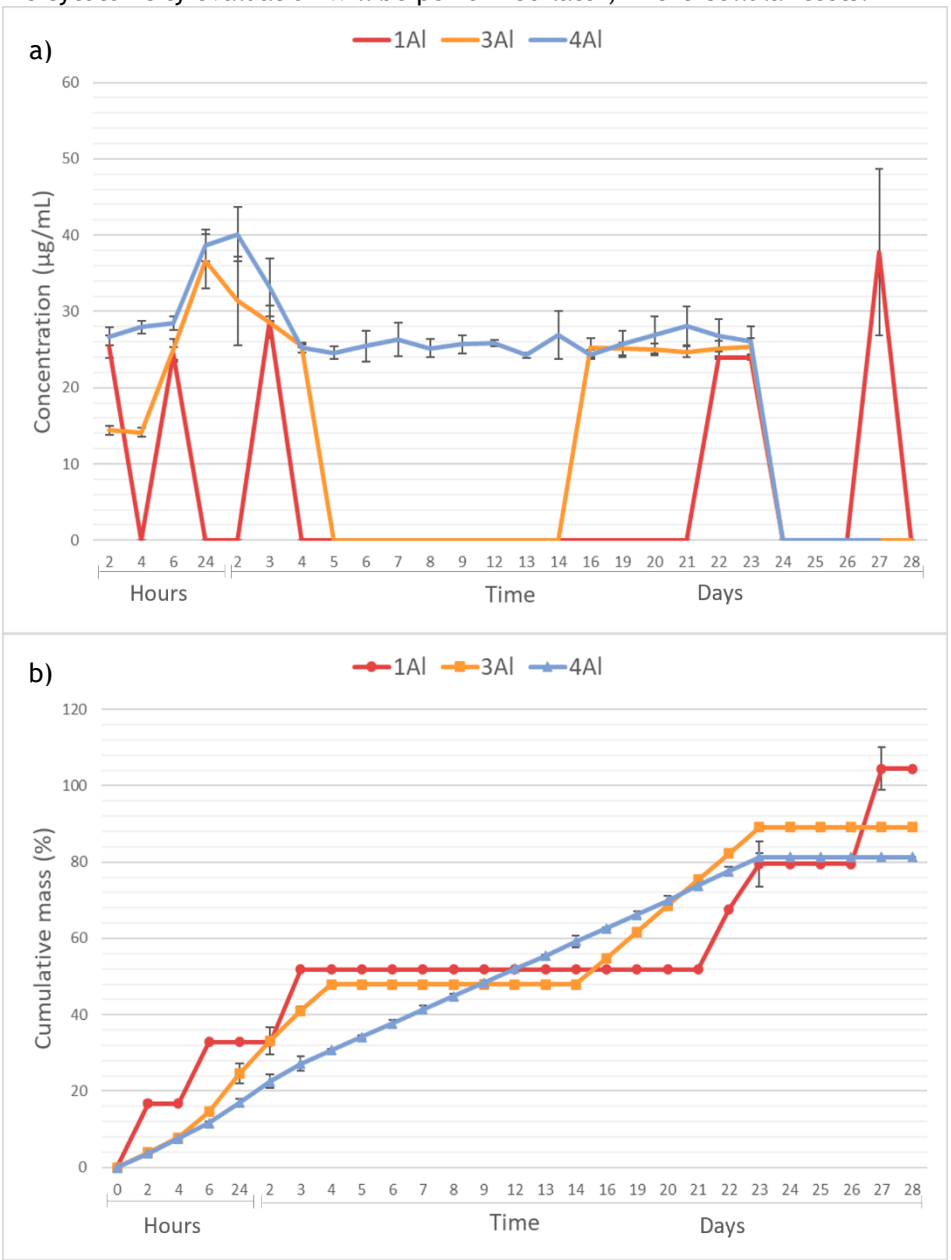


Figure 16- Alendronate concentration release profile (a) and cumulative mass percentage of alendronate released (b) in the 1Al, 3Al and 4Al conditions over 28 days.

4.3. Antibacterial activity assessment

To demonstrate the antibacterial ability of the spheres and validate the quantitative results obtained in the gentamicin release profiles, the agar diffusion test was performed in solid *Mueller Hinton* agar medium with the *S. aureus* ATCC 29213 bacterial strain. Since gentamicin also exhibits an inhibitory effect for gram-negative bacteria, it would also be pertinent to perform this test with a representative gram-negative bacterium, however, this was not attainable due to time constraints.

All of the dual loading conditions were used in this test to verify whether the release of the two drugs may interfere with each other. Additionally, spheres from the 1Al condition and non-loaded spheres were tested as a control. Therefore, it was expected that the spheres loaded with the two agents would exhibit an inhibitory halo while the spheres used as control would not.

4.3.1. Mueller Hinton agar diffusion test

As previously stated, *S. aureus* is the most common pathogenic bacterium causing bone infection. This bacterium can lead to severe bone loss and destruction upon infection. This is because, in the presence of *S. aureus*, osteoblasts become weaker upon infection and begin to undergo necrosis and apoptosis. Simultaneously, osteoclast proliferation and bone metabolic balance are disturbed, causing inflammatory bone loss [71]. Therefore, it is important that the porous spheres have an inhibitory capacity against this bacterium.

The results obtained in the agar diffusion test for the bacteria used are represented in figure 17. A significant inhibitory halo could be noticed on the first four days of the experiment, for all gentamicin-containing conditions (1G+1Al; 2G+1Al; 1G+3Al and 1G+4Al), being more prominent on the first two days, as expected given the quantitative gentamicin release results, discussed earlier. As anticipated, the two control conditions (1Al and non-loaded) never exhibited an inhibitory halo since no antibiotic was incorporated into these spheres, and both alendronate and alginate have no antibacterial properties. By the fourth and fifth days of the experiment, the inhibition halo was noticeably smaller, and by the sixth and seventh days, there was no inhibition halo. Nevertheless, despite the evident antibacterial effect of the spheres during five days, these results did not agree with the results obtained in the release kinetics, where the released values were above the minimum inhibitory concentration for the used bacteria (*S. aureus*) until the 16th day of the experiment. This can be explained by the fact that a concentration gradient is required for gentamicin to be released from the alginate network, meaning that there is an exchange of water molecules for gentamicin molecules in the hydrogel, causing the gentamicin to be released into the medium. Since the diffusion tests were performed in a solid medium, this driving force responsible for the release of gentamicin

(diffusion process) did not exist, making the release of this compound less pronounced, therefore, these experiments should be performed in a liquid medium rather than in a solid one. Furthermore, it is important to bear in mind that the obtained release profiles were only from individual conditions. In the bacterial experiments, double-loaded spheres were used, and as such, an extra barrier in the system interfered with the gentamicin diffusion.

The obtained results made it possible to state that the 2G+1Al condition did not present a significantly larger inhibitory halo than the remaining conditions, despite containing gentamicin at a higher concentration. Furthermore, it is also possible to imply that the presence of alendronate did not interfere with the antibacterial capacity of the spheres, as expected. Therefore, from the obtained results, it is possible to state that, for the intended application, the spheres from the 1G+1Al, 1G+3Al, and 1G+4Al conditions will be the best approaches since, even though they have a lower gentamicin concentration than the 2G+1Al one, they presented similar outcomes.

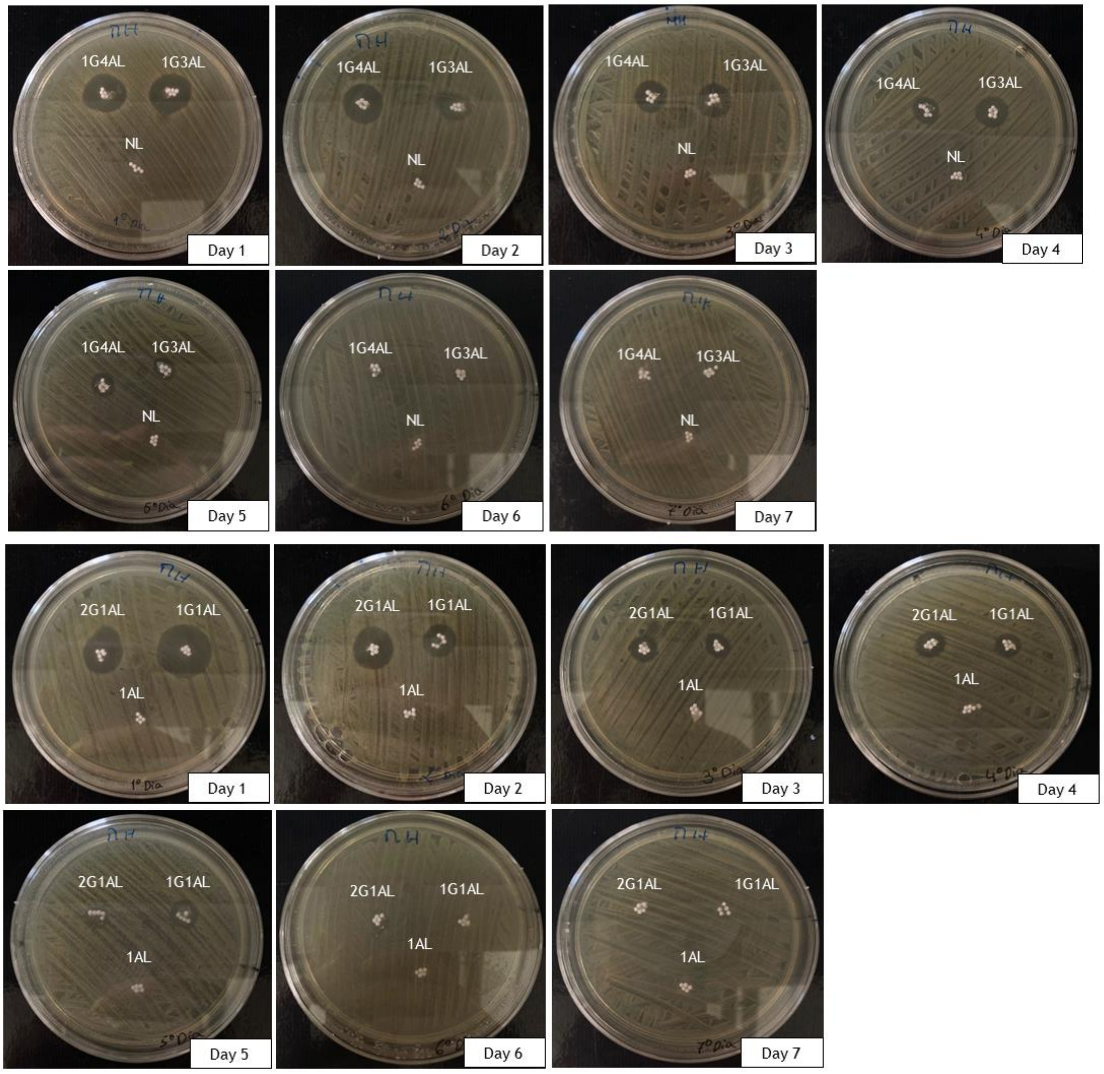


Figure 17- Bacterial tests on Mueller Hinton inoculated culture plates over 7 days. All dual loading conditions were tested (1G+4Al; 1G+3Al; 2G+1Al and 1G+1Al), as well as non-loaded and alendronate-loaded spheres (NL and 1Al).

4.4. *In Vitro* biological evaluation

In these experiments, human osteosarcoma cell lines (MG-63) were used as an osteoblastic model. As such, the biocompatibility of the dual-loaded and non-loaded (control) spheres was evaluated, as well as the cytotoxicity of different concentrations of alendronate. Regarding the spheres' experiment, samples from all the dual-loading conditions were used, except for the 1G+3Al condition. Since these were cytotoxicity assays, only the extreme conditions were tested.

As previously mentioned, reported studies in the literature have demonstrated that alendronate has been proven to inhibit bone resorption and induce mineralization of newly formed bone by osteoblasts. Recent studies also suggest that this compound enhances the osteogenic differentiation of osteoblasts and bone marrow mesenchymal stem cells [82]. Prior studies also indicate that alendronate boosted the synthesis of bone matrix proteins, osteocalcin, and collagen. These results show that bisphosphonates have considerable and direct impacts on osteogenesis in osteoblasts *in vitro*, in addition to their well-known effects on bone resorption [83].

To assess the metabolism of the seeded cells under different conditions, the resazurin assay was performed after 6h, 24h, 48h, 3, 4, 7, and 10 days of being seeded. This assay is based on the ability of viable, metabolically active cells to reduce resazurin to resorufin and dihydroresorufin. The resorufin produced from the reduction of resazurin is measured colorimetrically or fluorometrically; in this case, fluorometry was used. Resazurin is non-toxic to cells and is stable in a culture medium, allowing continuous measurement of cell metabolic activity *in vitro* as a kinetic or endpoint assay. The toxic effect that jeopardizes cell viability and proliferation also affects the ability of cultures to reduce resazurin, and the rate of reduction of the dye is directly proportional to cell viability. Therefore, the reduction of resazurin can provide an insight into the metabolic competence of the cells and thus their viability and proliferation [84].

4.4.1. Cytotoxicity evaluation of the samples

The results regarding the cytotoxicity evaluation of the spheres in the different conditions are represented in figure 18 in arbitrary fluorescence units (a.u.). It was possible to notice that the 1G+1Al condition stood out from the others, with the highest cell viability rate. As discussed in section 4.2.3, a few studies have reported that alendronate concentrations of 10^{-5} M or lower are ideal for osteoblast-like cell proliferation. In contrast, concentrations above 10^{-4} M are already decreasing cell viability [57], [85]. Now, when comparing these results with those from the release charts of the individual alendronate assays, in the 1Al condition, the release pulses observed in the chart are primarily in the 10^{-5} M range. On the other hand, in

the 4Al condition, the release pattern is relatively constant, and there were more time points where the release was at the threshold of cytotoxicity (10^{-4} M) for these cells. Therefore, the obtained cytotoxicity results meet with the release kinetics ones because, as anticipated, there was not as significant cell viability within the range of 10^{-4} M, while in the range of 10^{-5} M, there was a satisfactory cell viability rate. Even though the 2G+1Al condition has the same concentration of alendronate as the 1G+1Al one, the gentamicin concentration is higher. Therefore, as discussed in section 4.2.2.1, in the first few time points of the 2G condition, there was a release of gentamicin at higher concentrations than in the 1G sample. This resulted in a higher concentration of gentamicin in the release medium, which significantly decreased the concentration gradient in this system. Since alendronate diffuses similarly to gentamicin, a decrease in the concentration gradient of the system will not favor the diffusion of alendronate into the medium, which could translate into a decrease in osteoblast proliferation. This may explain that there was not such a pronounced cell proliferation in the 2G+1A condition. This is consistent with previous studies on hydrogels in drug delivery systems that reported that the flux of a given drug is proportional to the concentration gradient in the system [86].

From the obtained results, it was reasonable to assume that none of the tested conditions exhibited cytotoxicity for human osteosarcoma cells, when comparing with the control group. Given that the most extreme conditions were tested, it can also be presumed that the 1G+3Al condition would show no cytotoxicity for these cells.

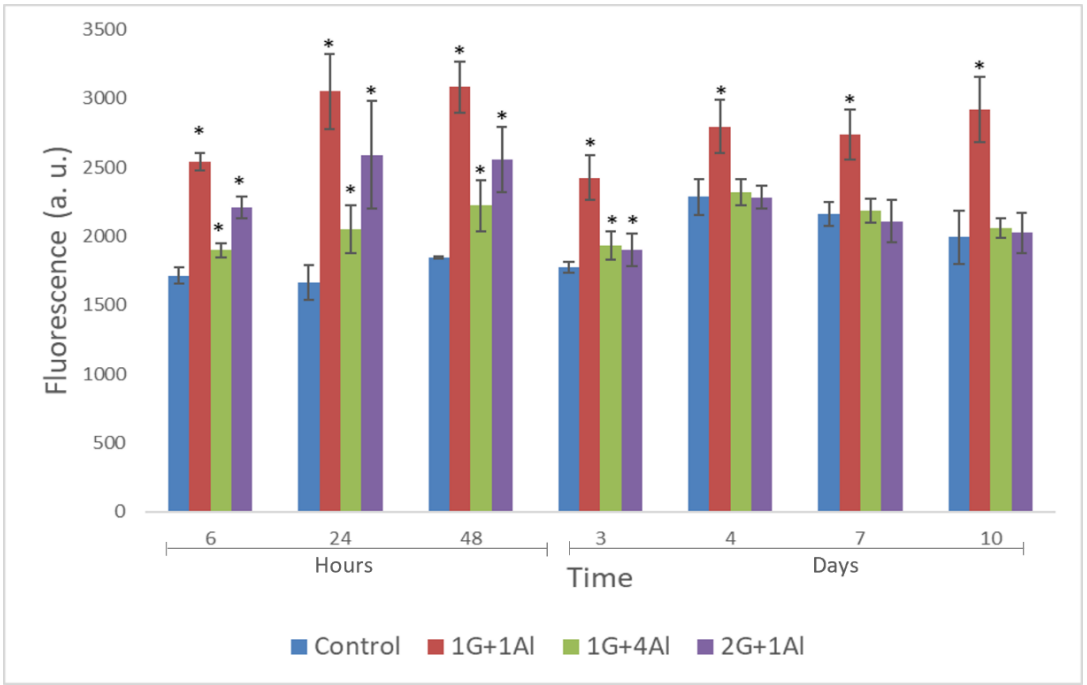


*Figure 18- Cytotoxicity of the 1G+1Al, 1G+4Al, 2G+1Al conditions and non-loaded spheres (control) over 10 days presented in fluorescence arbitrary units. *=p<0.05 between each sample and the control group at each time-point, for N=5.*

4.4.2. Cell morphology analysis

A prerequisite for cell bonding to a material's surface is naturally a set of appropriate surface characteristics, such as porosity or surface roughness. Cell attachment is the first stage of cell-material interactions, and the quality of this phase affects the capacity for cell proliferation and differentiation upon contact with the material. In addition, a few studies have demonstrated that material surfaces' chemical and topographic properties are of utmost importance, as they may influence cell behavior. An increased surface roughness significantly affects cell attachment and proliferation of human osteosarcoma MG-63 cell line, positively mediating cell adhesion, as reported in some studies [87]. Therefore, the SEM technique was employed to investigate cell morphology and its interactions with the material.

By observing figure 19, obtained by SEM, it was possible to note that at the 24-hour time point for the control group (figure 19a) there was some difficulty in spotting any cells. On the other hand, at 24 hours in the condition 1G+1Al (figure 19c) it was possible to observe, highlighted by the white arrows, spherically shaped MG-63 cells adhered to the sphere's surface and undergoing cell division. As for the 1G+4Al condition at 24 hours (figure 19e), it could be observed that the cells were in an elongated conformation with filopodial branches, signaled by the white arrows. In the 2G+1Al condition, at the 24-hour time point (figure 19g), it was possible to notice some cytoplasmic material on the surface of the alginate layer.

When observing the remaining images corresponding to the fourth day time point for the different conditions, there was difficulty in detecting cells in every condition. However, it was possible to find extracellular matrix debris in the samples (figure 19b, d, f, and h).

Based on these results and comparing them to the quantitative resazurin assay data, at 24 hours in the 1G+1Al condition was where more cells could be visualized, as expected. Within 24 hours of the 1G+4Al and 2G+1Al conditions, it was also possible to note some cells adhering to the material's surface, as expected from the results obtained in the resazurin assay.

By the third day of the resazurin assay, it was possible to notice a decline in cell viability in all tested conditions except for the control group as seen in figure 18. These outcomes are consistent with the qualitative SEM ones, whereby on the fourth day for all conditions, it was not feasible to observe cells, only cytoplasmic debris. This debris found on the sphere's surface indicated that the MG-63 cells had previously been adhered to the sphere and died, thus leaving cytoplasmic residues on the material. This phenomenon may be related to an increase in cell confluence around these time points (around the third and fourth days). Cell proliferation will ultimately lead to an increased cell confluence, defined as the ratio between the area occupied by the cells and the surface area of the cell culture. However, cell proliferation will decelerate or eventually cease when cell confluence becomes too high. Excessive cell confluence can result in a lack of nutrients and an accumulation of metabolites, leading to a decline in cell viability [88]. This explains the fact that after three days of the

experiment, there was a decline in cell viability resulting from cell death, and only extracellular matrix debris could be seen attached to the spheres in the SEM images.

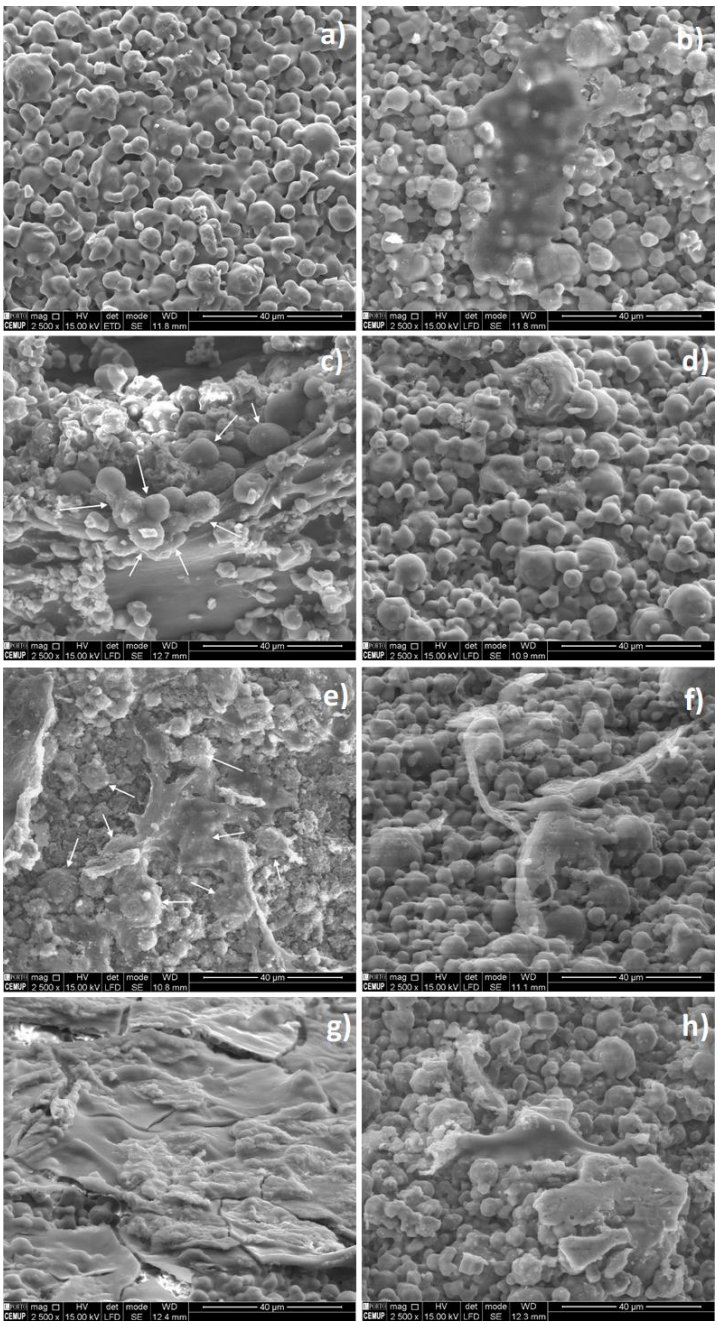


Figure 19- Images obtained using the SEM technique where cell-material interactions can be observed at 2500x magnification. Control group at 24 hours (a) and fourth day (b); 1G+1Al condition at 24 hours (c) and fourth day (d); 1G+4Al condition for 24 hours (e) and fourth day (f); 2G+1Al condition at 24 hours (g) and fourth day (h).

4.4.3. Cytotoxicity evaluation of the compound

The need to perform this experiment emerged from prior research, where it was found in several papers that concentrations of alendronate between 10^{-5} M and 10^{-11} M promote MG-63 cells proliferation, while concentrations of 10^{-4} M of the same compound inhibit it [57].

Therefore, the cytotoxicity of varying alendronate concentrations was also assessed using the resazurin assay. Additionally, cells were seeded onto treated plates suitable for cell culture and used as a positive control group. The results are represented in figure 20, in arbitrary fluorescence units. On the first and second days of the experiment, the cell viability of all conditions was quite similar, with no significant discrepancy between the values of fluorescence obtained. It was also noticeable that there was a considerable amount of fluorescence in the conditions of 10^{-4} M and 10^{-5} M concentration, which translates into good cellular metabolic activity and viability in these days. Starting on the fourth day of the experiment, an increase in fluorescence could be observed in the control group and the 10^{-6} M and 10^{-7} M conditions. Accompanied by a decrease in fluorescence in the 10^{-4} M and 10^{-5} M conditions. While the experiment was running, it was indeed possible to observe a pronounced change in the color of resazurin in the control group and in the 10^{-7} M condition, which also confirmed the results obtained since, according to the literature, resazurin is a purple, oxidation-reduction indicator that turns pink when cellular oxidoreductases reduce it to resorufin. Therefore, viable cell concentration in a suspension containing resazurin is reflected in the conversion from purple to pink color [89]. Based on the results, it was possible to state that there is some cytotoxicity of the compound at concentrations of 10^{-4} M and 10^{-5} M, which was the range of concentrations obtained in the alendronate release tests. This might be linked to the fact that the human osteosarcoma cell model (MG-63) was not the most suitable for this study, since, previous investigations have suggested that bisphosphonates induce tumor apoptosis of osteosarcoma cells in the range of concentrations of 10^{-4} M to 10^{-5} M, which might contribute to reducing the invasive potential of these tumor cells [90]. These cells are usually considered a suitable *in vitro* model to assess the biocompatibility of implanted materials. They were chosen because of their similarity to primary human osteoblasts, having the advantage of simple maintenance and an unlimited number of cells. However, these cells proved not to be suitable for this study [91]. Therefore, the best model to perform these biological assays would be mesenchymal stromal cells (MSCs) and evaluate their differentiation into osteoblastic cells.

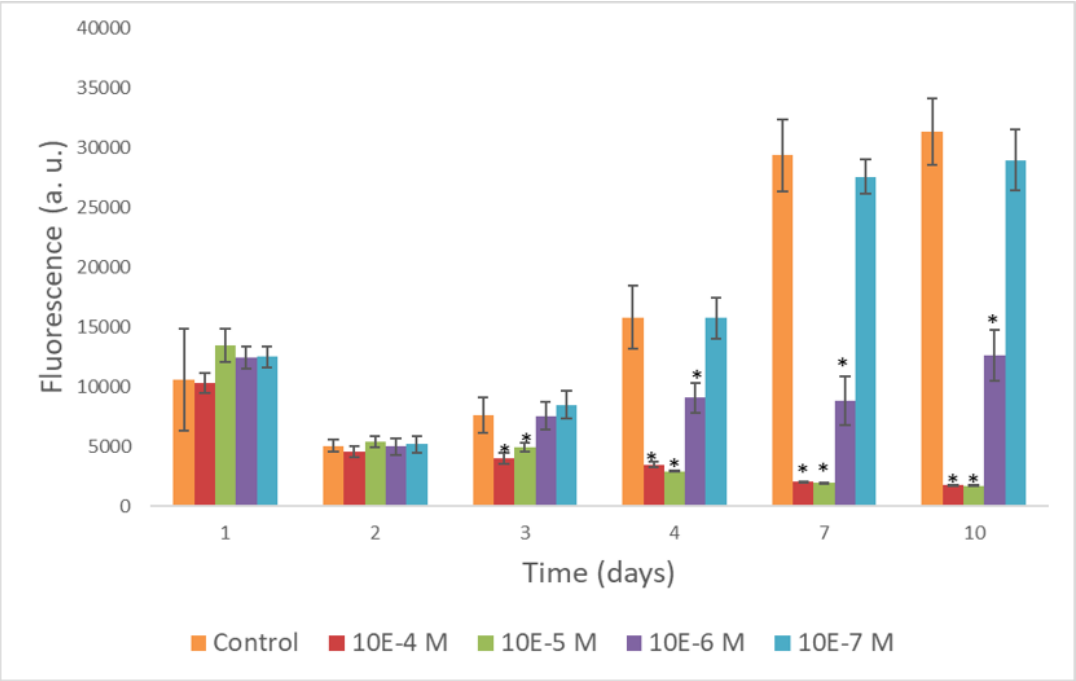


*Figure 20- Cytotoxicity of different concentrations of alendronate (10-4 M, 10-5 M,10-6 M,10-7 M) over 10 days presented in fluorescence arbitrary units. *=p<0.05 between each sample and the control group at each time-point, for N=5.*

Chapter 5: Conclusions and Future Work

The increasing average life expectancy and consequent population aging have led to a surge in musculoskeletal problems amongst the elderly. In recent years, the field of bone tissue regeneration has undergone remarkable development. However, no technique fully addresses the regenerative needs of bone tissue. Therefore, within the scope of this dissertation and in an attempt to overcome some limitations of the available bone substitutes, it was proposed to develop a system combining porous hollow hydroxyapatite spheres with an antibiotic and an osteogenic agent, with characteristics suitable for the release of these drugs. The spheres feature a hollow core destined for the incorporation of the alendronate. Conversely, the gentamicin is intended to be adsorbed onto the surface of the porous spheres along with the gelled alginate.

Within the experimental work itself, to ensure that the spheres had physical characteristics suitable for bone regeneration and drug release, a surfactant was used during the production of the spheres, which conferred on them a porosity and pore interconnectivity optimal for cell adhesion and proliferation as well as bone ingrowth.

Regarding the alendronate and gentamicin release studies, these were initially performed with spheres loaded with both agents and spheres loaded with just one of the drugs (gentamicin or alendronate). However, it became apparent that it was not feasible to quantify the drugs separately and so, in order to have an estimate of the drug release profile, only the individual conditions were quantified. Both agents presented a favorable drug loading efficiency in the porous spheres. Concerning the release profiles of gentamicin for both conditions tested, there was an initial release peak followed by a controlled release of the drug for around 17 days, which was around the desired drug release period. However, the 1G condition presented a higher amount of released drug after 17 days compared to the 2G one, which, for the intended application, indicates a more adequate release kinetics.

Regarding the alendronate release tests for the 1Al and 3Al conditions, these presented a markedly pulsatile profile, whereas, for a higher concentration administered (4Al condition), the release pattern was closer to stability. Within the context of the present study, having a pulsatile drug release pattern is a very promising aspect since a pulsatile drug release significantly promotes osteogenic differentiation through stimuli. Therefore, when comparing the release patterns of the three individual conditions tested, it can be stated that the 1Al condition has the highest therapeutic potential since it had the most pulsatile individual release profile, thus enhancing osteogenic differentiation.

Concerning the evaluation of the antibacterial effect of the spheres by the diffusion test in Mueller Hinton agar, the results indicated that all the spheres from conditions 1G+4Al, 1G+3Al, 1G+1Al, and 2G+1Al had an antibacterial effect for *S. aureus* over five days, without

significant differences. The discrepancy between these results and those of the gentamicin release studies may be because these tests were performed in a solid medium, which is not as conducive to gentamicin diffusion. Moreover, these experiments were performed with double-loaded spheres, which will obviously differ from the results obtained in the release profiles with spheres loaded only with gentamicin.

Regarding the cytotoxicity tests with MG-63 human osteosarcoma cells, it was observed that the 1G+1Al assay distinguished itself from the other conditions with the highest cell viability, making this condition the most suitable for the proliferation and differentiation of this type of cells, which was also possible to observe in the SEM images. As for the cytotoxicity assessment of different concentrations of alendronate, it could be concluded that there was some cytotoxicity of the compound at concentrations of 10^{-4} M and 10^{-5} M, which was the concentration range obtained in the alendronate release studies. This could be due to the fact that the human osteosarcoma cell model (MG-63) was not the most suitable for this study.

Given the results of all the experiments with both double-loaded and single-loaded spheres, it was possible to conclude that the condition with the most potential for the intended application is 1G+1Al. However, some future work is suggested in order to improve the experimental approach.

Some further work that should be implemented in the drug release studies is accurately quantifying the two compounds in double-loaded spheres using the high-performance liquid chromatography technique. This will allow an accurate quantification of the dual release profiles of gentamicin and alendronate, which will possibly differ from when the spheres are loaded with only one compound. In the present study, the drug release was evaluated using a static system, which does not accurately reflect *in vivo* circumstances where physiological fluid flow is continuous. Therefore, in further research, it would be crucial to carry out these tests in a dynamic system with simulated body fluid. Additionally, to obtain more reliable gentamicin diffusion results when evaluating the antibacterial effect of the spheres, these should be performed in a liquid medium rather than a solid medium, not only because the liquid medium will promote the gentamicin diffusion but also because it mimics what will happen in a physiological environment following the spheres' implantation. As previously stated, gentamicin is an antibiotic with an activity spectrum against both gram-positive and gram-negative bacteria and therefore it would also be relevant to perform these assays with a representative gram-negative bacterium, such as, *Escherichia coli* or *Pseudomonas aeruginosa*.

Moreover, the concentration range of alendronate released by the spheres is borderline cytotoxic for MG-63 cells. Thus, it would be interesting to reduce the concentration of alendronate administered to the spheres and perform *in vitro* biological tests with mesenchymal stromal cells (MSCs) to evaluate their differentiation into osteoblasts, by analyzing osteoblast differentiation markers, such as alkaline phosphatase. Furthermore, to commercialize the product in the future, once all the *in vitro* tests have been optimized, *in*

vivo tests should be performed, preferably in a sheep model, for the required bone regeneration time and follow-up should be done, using, for example, x-ray analysis and histological studies. Finally, clinical trials will need to be conducted.

References

[1] M. R. Report, “Bone Grafts and Substitutes Market - Growth, Trends, COVID-19 Impact, and Forecasts (2022 - 2027),” 2022. https://www.giiresearch.com/report/moi925218-bone-grafts-substitutes-market-growth-trends.html (accessed Aug. 30, 2022).

[2] A. J. Salgado, O. P. Coutinho, and R. L. Reis, “Bone tissue engineering: State of the art and future trends,” *Macromol. Biosci.*, vol. 4, no. 8, pp. 743–765, 2004, doi: 10.1002/mabi.200400026.

[3] J. J. Li, M. Ebied, J. Xu, and H. Zreiqat, “Current Approaches to Bone Tissue Engineering: The Interface between Biology and Engineering,” *Adv. Healthc. Mater.*, vol. 7, no. 6, pp. 1–8, 2018, doi: 10.1002/adhm.201701061.

[4] I. Uçkay, P. Hoffmeyer, D. Lew, and D. Pittet, “Prevention of surgical site infections in orthopaedic surgery and bone trauma: State-of-the-art update,” *J. Hosp. Infect.*, vol. 84, no. 1, pp. 5–12, 2013, doi: 10.1016/j.jhin.2012.12.014.

[5] G. Q. Li, F. F. Guo, Y. Ou, G. W. Dong, and W. Zhou, “Epidemiology and outcomes of surgical site infections following orthopedic surgery,” *Am. J. Infect. Control*, vol. 41, no. 12, pp. 1268–1271, 2013, doi: 10.1016/j.ajic.2013.03.305.

[6] B. Clarke, “Normal bone anatomy and physiology.,” *Clin. J. Am. Soc. Nephrol.*, vol. 3 Suppl 3, pp. 131–139, 2008, doi: 10.2215/CJN.04151206.

[7] A. L. Boskey, “Bone composition: relationship to bone fragility and antiosteoporotic drug effects,” *Bonekey Rep.*, vol. 2, no. July, pp. 1–11, 2013, doi: 10.1038/bonekey.2013.181.

[8] A. Mallorie and B. Shine, “Normal bone physiology, remodelling and its hormonal regulation,” *Surg. (United Kingdom)*, vol. 40, no. 3, pp. 163–168, 2022, doi: 10.1016/j.mpsur.2021.12.001.

[9] T. A. Einhorn, “The cell and molecular biology of fracture healing,” *Clin. Orthop. Relat. Res.*, vol. 355, no. SUPPL., pp. 7–21, 1998, doi: 10.1097/00003086-199810001-00003.

[10] R. A. D. Carano and E. H. Filvaroff, “Angiogenesis and bone repair,” *Drug Discov. Today*, vol. 8, no. 21, pp. 980–989, 2003, doi: 10.1016/S1359-6446(03)02866-6.

[11] K. Arvidson *et al.*, “Bone regeneration and stem cells,” *J. Cell. Mol. Med.*, vol. 15, no. 4, pp. 718–746, 2011, doi: 10.1111/j.1582-4934.2010.01224.x.

[12] H. F. Pereira, I. F. Cengiz, F. S. Silva, R. L. Reis, and J. M. Oliveira, “Scaffolds and coatings for bone regeneration,” *J. Mater. Sci. Mater. Med.*, vol. 31, no. 3, 2020, doi: 10.1007/s10856-020-06364-y.

[13] H. Tal, “Bone Regeneration,” InTech, 2012, pp. 13–14.

[14] M. Barry, H. Pearce, L. Cross, M. Tatullo, and A. K. Gaharwar, “Advances in Nanotechnology for the Treatment of Osteoporosis,” *Curr. Osteoporos. Rep.*, vol. 14, no. 3, pp. 87–94, 2016, doi: 10.1007/s11914-016-0306-3.

[15] L. Jiliang, M. A. Kacena, and D. L. Stocum, “Chapter 12 - Fracture Healing,” in *Basic and Applied Bone Biology*, Second., B. David B. and A. Matthew R., Eds. 2019, pp. 235–253.

[16] T. Sozen, L. Ozisik, and N. Calik Basaran, “An overview and management of osteoporosis,” *Eur. J. Rheumatol.*, vol. 4, no. 1, pp. 46–56, 2017, doi: 10.5152/eurjrheum.2016.048.

[17] N. I. of H. NIH, “National Institutes of Health (NIH) Consensus Development Panel on Osteoporosis Prevention, Diagnosis, and Therapy,” *Jama*, vol. 285, no. 6, pp. 785–795, 2001.

[18] T. D. Rachner, S. Khosla, and L. C. Hofbauer, “Osteoporosis: Now and the future,” *Lancet*, vol. 377, no. 9773, pp. 1276–1287, 2011, doi: 10.1016/S0140-6736(10)62349-5.

[19] A. Bigham-Sadegh and A. Oryan, “Basic concepts regarding fracture healing and the current options and future directions in managing bone fractures,” *Int. Wound J.*, vol. 12, no. 3, pp. 238–247, 2015, doi: 10.1111/iwj.12231.

[20] E. H. Schemitsch, “Size Matters: Defining Critical in Bone Defect Size!,” *J. Orthop. Trauma*, vol. 31, no. 5, pp. S20–S22, Oct. 2017, doi: 10.1097/BOT.0000000000000978.

[21] W. Elshahawy, “Biocompatibility,” in *Advances in Ceramics - Electric and Magnetic*

Ceramics, Bioceramics, Ceramics and Environment, InTech, 2011.
[22] V. KARAGEORGIOU and D. KAPLAN, "Porosity of 3D biomaterial scaffolds and osteogenesis," *Biomaterials*, vol. 26, no. 27, pp. 5474–5491, Sep. 2005, doi: 10.1016/j.biomaterials.2005.02.002.
[23] X. Wang, J.-M. Ruan, and Q.-Y. Chen, "Effects of surfactants on the microstructure of porous ceramic scaffolds fabricated by foaming for bone tissue engineering," *Mater. Res. Bull.*, vol. 44, no. 6, pp. 1275–1279, Jun. 2009, doi: 10.1016/j.materresbull.2009.01.004.
[24] J. R. Woodard *et al.*, "The mechanical properties and osteoconductivity of hydroxyapatite bone scaffolds with multi-scale porosity," *Biomaterials*, vol. 28, no. 1, pp. 45–54, Jan. 2007, doi: 10.1016/j.biomaterials.2006.08.021.
[25] S. T. Moore *et al.*, "Osteoconductivity and Osteoinductivity of Puros® DBM Putty," *J. Biomater. Appl.*, vol. 26, no. 2, pp. 151–171, Aug. 2011, doi: 10.1177/0885328210366061.
[26] Y. Fillingham and J. Jacobs, "Bone grafts and their substitutes," *Bone Joint J.*, vol. 98-B, no. 1_Supple_A, pp. 6–9, Jan. 2016, doi: 10.1302/0301-620X.98B.36350.
[27] W. Wang and K. W. K. Yeung, "Bone grafts and biomaterials substitutes for bone defect repair: A review," *Bioact. Mater.*, vol. 2, no. 4, pp. 224–247, Dec. 2017, doi: 10.1016/j.bioactmat.2017.05.007.
[28] W. R. Moore, S. E. Graves, and G. I. Bain, "Synthetic bone graft substitutes," *ANZ J. Surg.*, vol. 71, no. 6, pp. 354–361, Jun. 2001, doi: 10.1046/j.1440-1622.2001.02128.x.
[29] A. J. Salinas, P. Esbrit, and M. Vallet-Regí, "A tissue engineering approach based on the use of bioceramics for bone repair," *Biomater. Sci.*, vol. 1, no. 1, pp. 40–51, 2013, doi: 10.1039/C2BM00071G.
[30] A. El-Ghannam, "Bone reconstruction: from bioceramics to tissue engineering," *Expert Rev. Med. Devices*, vol. 2, no. 1, pp. 87–101, Jan. 2005, doi: 10.1586/17434440.2.1.87.
[31] D. Bellucci, A. Sola, and V. Cannillo, "Hydroxyapatite and tricalcium phosphate composites with bioactive glass as second phase: State of the art and current applications," *J. Biomed. Mater. Res. Part A*, vol. 104, no. 4, pp. 1030–1056, Apr. 2016, doi: 10.1002/jbm.a.35619.
[32] E. Sarigol-Calamak and C. Hascicek, "Tissue Scaffolds As a Local Drug Delivery System for Bone Regeneration," 2018, pp. 475–493.
[33] E. Verron, J. M. Bouler, and J. Guicheux, "Controlling the biological function of calcium phosphate bone substitutes with drugs," *Acta Biomater.*, vol. 8, no. 10, pp. 3541–3551, Oct. 2012, doi: 10.1016/j.actbio.2012.06.022.
[34] R. Dorati *et al.*, "Biodegradable Scaffolds for Bone Regeneration Combined with Drug-Delivery Systems in Osteomyelitis Therapy," *Pharmaceuticals*, vol. 10, no. 4, p. 96, Dec. 2017, doi: 10.3390/ph10040096.
[35] T. R. Hoare and D. S. Kohane, "Hydrogels in drug delivery: Progress and challenges," *Polymer (Guildf).*, vol. 49, no. 8, pp. 1993–2007, Apr. 2008, doi: 10.1016/j.polymer.2008.01.027.
[36] B. Aderibigbe, I. Aderibigbe, and P. Popoola, "Design and biological evaluation of delivery systems containing bisphosphonates," *Pharmaceutics*, vol. 9, no. 1, pp. 1–24, 2017, doi: 10.3390/pharmaceutics9010002.
[37] C. L. McDonald, N. J. Lemme, E. J. Testa, R. Aaron, D. A. Hartnett, and E. M. Cohen, "Bisphosphonates in Total Joint Arthroplasty: A Review of Their Use and Complications," *Arthroplast. Today*, vol. 14, pp. 133–139, Apr. 2022, doi: 10.1016/j.artd.2022.02.003.
[38] M. Fazil, S. Baboota, J. K. Sahni, Ameeduzzafar, and J. Ali, "Bisphosphonates: therapeutics potential and recent advances in drug delivery," *Drug Deliv.*, vol. 22, no. 1, pp. 1–9, Jan. 2015, doi: 10.3109/10717544.2013.870259.
[39] C. Zhao, W. Liu, M. Zhu, C. Wu, and Y. Zhu, "Bioceramic-based scaffolds with antibacterial function for bone tissue engineering: A review," *Bioact. Mater.*, vol. 18, no. January, pp. 383–398, 2022, doi: 10.1016/j.bioactmat.2022.02.010.
[40] K. Kanellakopoulou and E. J. Giamarellos-Bourboulis, "Carrier Systems for the Local Delivery of Antibiotics in Bone Infections," *Drugs*, vol. 59, no. 6, pp. 1223–1232, Jun. 2000, doi: 10.2165/00003495-200059060-00003.
[41] J. Jackson, J. Lo, E. Hsu, H. M. Burt, A. Shademani, and D. Lange, "The Combined Use of Gentamicin and Silver Nitrate in Bone Cement for a Synergistic and Extended

Antibiotic Action against Gram-Positive and Gram-Negative Bacteria," *Materials (Basel).*, vol. 14, no. 12, p. 3413, Jun. 2021, doi: 10.3390/ma14123413.

[42] K. S. Hamilton, K. V. Gopal, E. J. Moore, and G. W. Gross, "Pharmacological response sensitization in nerve cell networks exposed to the antibiotic gentamicin," *Eur. J. Pharmacol.*, vol. 794, pp. 92–99, Jan. 2017, doi: 10.1016/j.ejphar.2016.11.017.

[43] C. E. Gillman and A. C. Jayasuriya, "FDA-approved bone grafts and bone graft substitute devices in bone regeneration," *Mater. Sci. Eng. C*, vol. 130, no. February, p. 112466, 2021, doi: 10.1016/j.msec.2021.112466.

[44] M. Cámara-Torres *et al.*, "3D additive manufactured composite scaffolds with antibiotic-loaded lamellar fillers for bone infection prevention and tissue regeneration," *Bioact. Mater.*, vol. 6, no. 4, pp. 1073–1082, 2021, doi: 10.1016/j.bioactmat.2020.09.031.

[45] A. Bow, D. E. Anderson, and M. Dhar, "Commercially available bone graft substitutes: the impact of origin and processing on graft functionality," *Drug Metab. Rev.*, vol. 51, no. 4, pp. 533–544, 2019, doi: 10.1080/03602532.2019.1671860.

[46] I. Sallent *et al.*, "The Few Who Made It: Commercially and Clinically Successful Innovative Bone Grafts," *Front. Bioeng. Biotechnol.*, vol. 8, no. September, pp. 1–8, 2020, doi: 10.3389/fbioe.2020.00952.

[47] M. Hallman and A. Thor, "Bone substitutes and growth factors as an alternative / complement to autogenous bone for grafting in implant dentistry," *Periodontol. 2000*, vol. 47, 2008.

[48] Leader Biomedical, "A comprehensive bone cement portfolio for joint replacement and joint revision," 2022. https://www.leaderbiomedical.com/products/c-ment-pmma-bone-cement/ (accessed Sep. 04, 2022).

[49] Heraeus Medical, "PALACOS® +G*: Antibiotic Loaded Bone Cements," 2022. https://www.heraeus.com/us/hme/usa_products_heraeus_medical/us_palacos_bone_cements/palacos_antibiotic_loaded_bone_cement/palacos_with_gentamicin.html (accessed Sep. 04, 2022).

[50] © DePuy Synthes, "DePuy CMW™ Heritage Bone Cements," 2016. https://5.imimg.com/data5/YR/IH/MY-62341139/depuy-cmw-1-bone-cement.pdf (accessed Sep. 04, 2022).

[51] Heraeus Medical, "PALAMED Bone cements for vacuum mixing without prior cooling," 2019. https://mti.mt-intl.ro/wp-content/uploads/2019/06/bro_Palamed_EN.pdf (accessed Sep. 05, 2022).

[52] Stryker, "Simplex Bone Cement," 2022. https://www.strykermeded.com/medical-devices/surgical-solutions/surgical-equipment/simplex-bone-cement/ (accessed Sep. 05, 2022).

[53] X. Kuang, G. Carotenudo, and L. Nicolais, "A Review of Ceramic Sintering and Suggestions on Reducing Sintering Temperatures," Naples, 1997.

[54] K. A. HING, S. M. BEST, and W. BONFIELD, "Characterization of porous hydroxyapatite," *J. Mater. Sci. Mater. Med. 1 0*, 1999, doi: https://doi.org/10.1023/A:1008929305897.

[55] W. Zhou, R. P. Apkarian, Z. L. Wang, and D. Joy, "Fundamentals of Scanning Electron Microscopy (SEM)," in *Scanning microscopy for nanotechnology*, New York: Springer, 2006, pp. 1–40.

[56] Y.-H. Kim and Y. Tabata, "Dual-controlled release system of drugs for bone regeneration," *Adv. Drug Deliv. Rev.*, vol. 94, pp. 28–40, Nov. 2015, doi: 10.1016/j.addr.2015.06.003.

[57] Y. Xiong, H. J. Yang, J. Feng, Z. L. Shi, and L. D. Wu, "Effects of alendronate on the proliferation and osteogenic differentiation of MG-63 cells," *J. Int. Med. Res.*, vol. 37, no. 2, pp. 407–416, 2009, doi: 10.1177/147323000903700216.

[58] M. S. H. Akash, K. Rehman, and S. Chen, "Pluronic F127-Based Thermosensitive Gels for Delivery of Therapeutic Proteins and Peptides," *Polym. Rev.*, vol. 54, no. 4, pp. 573–597, Oct. 2014, doi: 10.1080/15583724.2014.927885.

[59] B. Kundu *et al.*, "Development of porous HAp and β-TCP scaffolds by starch consolidation with foaming method and drug-chitosan bilayered scaffold based drug delivery system," *J. Mater. Sci. Mater. Med.*, vol. 21, no. 11, pp. 2955–2969, Nov. 2010, doi: 10.1007/s10856-010-4127-0.

[60] N. Abbasi, S. Hamlet, R. M. Love, and N.-T. Nguyen, "Porous scaffolds for bone

regeneration," *J. Sci. Adv. Mater. Devices*, vol. 5, no. 1, pp. 1–9, Mar. 2020, doi: 10.1016/j.jsamd.2020.01.007.
[61] J. Unosson, E. B. Montufar, H. Engqvist, M. P. Ginebra, and C. Persson, "Brushite foams - The effect of Tween® 80 and Pluronic® F-127 on foam porosity and mechanical properties," *J. Biomed. Mater. Res. - Part B Appl. Biomater.*, vol. 104, no. 1, pp. 67–77, 2016, doi: 10.1002/jbm.b.33355.
[62] C. M. Murphy, M. G. Haugh, and F. J. O'Brien, "The effect of mean pore size on cell attachment, proliferation and migration in collagen–glycosaminoglycan scaffolds for bone tissue engineering," *Biomaterials*, vol. 31, no. 3, pp. 461–466, Jan. 2010, doi: 10.1016/j.biomaterials.2009.09.063.
[63] P. Mohazzab, "Archimedes' Principle Revisited," *J. Appl. Math. Phys.*, vol. 05, no. 04, pp. 836–843, 2017, doi: 10.4236/jamp.2017.54073.
[64] J. R. Jones and L. L. Hench, "Regeneration of trabecular bone using porous ceramics," *Curr. Opin. Solid State Mater. Sci.*, vol. 7, no. 4–5, pp. 301–307, Aug. 2003, doi: 10.1016/j.cossms.2003.09.012.
[65] C. C. Coelho, R. Araújo, P. A. Quadros, S. R. Sousa, and F. J. Monteiro, "Antibacterial bone substitute of hydroxyapatite and magnesium oxide to prevent dental and orthopaedic infections," *Mater. Sci. Eng. C*, vol. 97, no. December 2018, pp. 529–538, 2019, doi: 10.1016/j.msec.2018.12.059.
[66] Transparency market research, "Surgical Site Infection (SSI) Market - Global Industry Analysis, Size, Share, Growth, Trends and Forecast 2019 - 2027." https://www.transparencymarketresearch.com/surgical-site-infection-market.html (accessed Jun. 06, 2022).
[67] OECD, "Healthe at a Glance: Europe 2018," 2018, p. 2.
[68] F. A. Al-Mulhim, M. A. Baragbah, M. Sadat-Ali, A. S. Alomran, and M. Q. Azam, "Prevalence of surgical site infection in orthopedic surgery: A 5-year analysis," *Int. Surg.*, vol. 99, no. 3, pp. 264–268, 2014, doi: 10.9738/INTSURG-D-13-00251.1.
[69] M. Ribeiro, F. J. Monteiro, and M. P. Ferraz, "Infection of orthopedic implants with emphasis on bacterial adhesion process and techniques used in studying bacterial-material interactions," *Biomatter*, vol. 2, no. 4, pp. 176–194, Oct. 2012, doi: 10.4161/biom.22905.
[70] R. Dorati *et al.*, "Biodegradable scaffolds for bone regeneration combined with drug-delivery systems in osteomyelitis therapy," *Pharmaceuticals*, vol. 10, no. 4, 2017, doi: 10.3390/ph10040096.
[71] Q. Wen, F. Gu, Z. Sui, Z. Su, and T. Yu, "The Process of Osteoblastic Infection by Staphylococcus Aureus," *Int. J. Med. Sci.*, vol. 17, no. 10, pp. 1327–1332, 2020, doi: 10.7150/ijms.45960.
[72] G. A. Noskin *et al.*, "The Burden of Staphylococcus aureus Infections on Hospitals in the United States," *Arch. Intern. Med.*, vol. 165, no. 15, p. 1756, Aug. 2005, doi: 10.1001/archinte.165.15.1756.
[73] A. L. Baltch, W. J. Ritz, L. H. Bopp, P. B. Michelsen, and R. P. Smith, "Antimicrobial Activities of Daptomycin, Vancomycin, and Oxacillin in Human Monocytes and of Daptomycin in Combination with Gentamicin and/or Rifampin in Human Monocytes and in Broth against Staphylococcus aureus," *Antimicrob. Agents Chemother.*, vol. 51, no. 4, pp. 1559–1562, Apr. 2007, doi: 10.1128/AAC.00973-06.
[74] C.-H. David Chen, C.-C. Chen, M.-Y. Shie, C.-H. Huang, and S.-J. Ding, "Controlled release of gentamicin from calcium phosphate/alginate bone cement," *Mater. Sci. Eng. C*, vol. 31, no. 2, pp. 334–341, Mar. 2011, doi: 10.1016/j.msec.2010.10.002.
[75] A. El-Ghannam, K. Ahmed, and M. Omran, "Nanoporous delivery system to treat osteomyelitis and regenerate bone: Gentamicin release kinetics and bactericidal effect," *J. Biomed. Mater. Res. Part B Appl. Biomater.*, vol. 73B, no. 2, pp. 277–284, May 2005, doi: 10.1002/jbm.b.30209.
[76] H. H. Tønnesen and J. Karlsen, "Alginate in drug delivery systems," *Drug Dev. Ind. Pharm.*, vol. 28, no. 6, pp. 621–630, 2002, doi: 10.1081/DDC-120003853.
[77] N. H. Golden *et al.*, "Alendronate for the Treatment of Osteopenia in Anorexia Nervosa: A Randomized, Double-Blind, Placebo-Controlled Trial," *J. Clin. Endocrinol. Metab.*, vol. 90, no. 6, pp. 3179–3185, Jun. 2005, doi: 10.1210/jc.2004-1659.
[78] V. Breuil *et al.*, "Human Osteoclast Formation and Activity In Vitro: Effects of

Alendronate," *J. Bone Miner. Res.*, vol. 13, no. 11, pp. 1721–1729, Nov. 1998, doi: 10.1359/jbmr.1998.13.11.1721.

[79] L. Che *et al.*, "A biomimetic and bioactive scaffold with intelligently pulsatile teriparatide delivery for local and systemic osteoporosis regeneration," *Bioact. Mater.*, vol. 19, pp. 75–87, Jan. 2023, doi: 10.1016/j.bioactmat.2022.03.023.

[80] R. A. Siegel and M. J. Rathbone, "Overview of Controlled Release Mechanisms," in *Fundamentals and Applications of Controlled Release Drug Delivery*, Boston, MA: Springer US, 2012, pp. 19–43.

[81] H.-J. Moon *et al.*, "Effect of heparin and alendronate coating on titanium surfaces on inhibition of osteoclast and enhancement of osteoblast function," *Biochem. Biophys. Res. Commun.*, vol. 413, no. 2, pp. 194–200, Sep. 2011, doi: 10.1016/j.bbrc.2011.08.057.

[82] S. E. Kim *et al.*, "Local delivery of alendronate eluting chitosan scaffold can effectively increase osteoblast functions and inhibit osteoclast differentiation," *J. Mater. Sci. Mater. Med.*, vol. 23, no. 11, pp. 2739–2749, Nov. 2012, doi: 10.1007/s10856-012-4729-9.

[83] M. Tsuchimoto *et al.*, "Alendronate Modulates Osteogenesis of Human Osteoblastic Cells In Vitro," *Jpn. J. Pharmacol.*, vol. 66, no. 1, pp. 25–34, 1994, doi: 10.1254/jjp.66.25.

[84] S. Anoopkumar-Dukie, J. B. Carey, T. Conere, E. O'Sullivan, F. N. van Pelt, and A. Allshire, "Resazurin assay of radiation response in cultured cells," *Br. J. Radiol.*, vol. 78, no. 934, pp. 945–947, Oct. 2005, doi: 10.1259/bjr/54004230.

[85] C. García-Moreno *et al.*, "Effect of alendronate on cultured normal human osteoblasts," *Bone*, vol. 22, no. 3, pp. 233–239, Mar. 1998, doi: 10.1016/S8756-3282(97)00270-6.

[86] F. Bierbrauer, "Hydrogel Drug Delivery: Diffusion Models." 2005.

[87] N. K. Nguyen, M. Leoni, D. Maniglio, and C. Migliaresi, "Hydroxyapatite nanorods: Soft-template synthesis, characterization and preliminary in vitro tests," *J. Biomater. Appl.*, vol. 28, no. 1, pp. 49–61, Jul. 2013, doi: 10.1177/0885328212437065.

[88] H. Bai, C. Lu, M. Ma, S. Yan, J. Zhang, and Z. Han, "An improved U-Net for cell confluence estimation," *Optoelectron. Lett.*, vol. 18, no. 6, pp. 378–384, Jun. 2022, doi: 10.1007/s11801-022-1129-3.

[89] D. A. Hudman and N. J. Sargentini, "Resazurin-based assay for screening bacteria for radiation sensitivity," *Springerplus*, vol. 2, no. 1, p. 55, Dec. 2013, doi: 10.1186/2193-1801-2-55.

[90] Y. Y. Cheng, L. Huang, K. M. Lee, K. Li, and S. M. Kumta, "Alendronate regulates cell invasion and MMP-2 secretion in human osteosarcoma cell lines," *Pediatr. Blood Cancer*, vol. 42, no. 5, pp. 410–415, May 2004, doi: 10.1002/pbc.20019.

[91] S. Staehlke, H. Rebl, and B. Nebe, "Phenotypic stability of the human MG-63 osteoblastic cell line at different passages," *Cell Biol. Int.*, vol. 43, no. 1, pp. 22–32, Jan. 2019, doi: 10.1002/cbin.11073.